

Hyperaccreting Neutron-Star Disks and Neutrino Annihilation

Dong Zhang and Z. G. Dai

Department of Astronomy, Nanjing University, Nanjing 210093, China;
dongzhanghz@gmail.com, dzg@nju.edu.cn

ABSTRACT

Newborn neutron stars surrounded by hyperaccreting and neutrino-cooled disks may exist in some gamma-ray bursts (GRBs) and/or supernovae (SNe). In this paper we further study the structure of such a neutron-star disk based on the two-region (i.e., inner & outer) disk scenario following our previous work, and calculate the neutrino annihilation luminosity from the disk in various cases. We investigate the effects of the viscosity parameter α , energy parameter ε (measuring the neutrino cooling efficiency of the inner disk) and outflow strength on the structure of the entire disk as well as the effect of emission from the neutron star surface boundary emission on the total neutrino annihilation rate. The inner disk satisfies the entropy-conservation self-similar structure for the energy parameter $\varepsilon \simeq 1$ and the advection-dominated structure for $\varepsilon < 1$. An outflow from the disk decreases the density and pressure but increases the thickness of the disk. Moreover, compared with the black-hole disk, the neutrino annihilation luminosity above the neutron-star disk is higher, and the neutrino emission from the boundary layer could increase the neutrino annihilation luminosity by about one order of magnitude higher than the disk without boundary emission. The neutron-star disk with the advection-dominated inner disk could produce the highest neutrino luminosity while the disk with an outflow has the lowest. Although a heavily mass-loaded outflow from the neutron star surface at early times of neutron star formation prevents the outflow material from being accelerated to a high bulk Lorentz factor, an energetic ultrarelativistic jet via neutrino annihilation can be produced above the stellar polar region at late times if the disk accretion rate and the neutrino emission luminosity from the surface boundary layer are sufficiently high.

Subject headings: accretion: accretion disks — black holes — gamma rays: bursts — neutrinos — stars: neutron

1. Introduction

The hyperaccreting disk surrounding a stellar-mass black hole possibly formed by the merger of a compact object binary or the collapse of a massive star has been argued to be a candidate for central engines of gamma-ray bursts (GRBs) (e.g. Eichler et al. 1989; Narayan et al. 1992; Woosley 1993; Paczyński 1998; Popham et al. 1999; MacFadyen & Woosley 1999; Narayan et al. 2001). The typical mass of the debris dense torus or disk is about $0.01 - 1M_{\odot}$ with large angular momentum as well as high accretion rate up to $\sim 1.0M_{\odot} \text{ s}^{-1}$. Although the optical depth of the accreting matter in the disk is enormous, the disk can be cooled or partly cooled via neutrino emission. A number of studies have investigated the structure and energy transfer of the neutrino-cooled disk around a black hole both in steady-state and time-dependent considerations over last several years (Popham et al. 1999; Narayan et al. 2001; Kohri & Mineshige 2002; Di Matteo et al. 2002; Kohri et al. 2005; Gu et al. 2006; Kawanaka & Mineshige 2007; Chen & Beloborodov 2007; Liu et al. 2007; Janiuk et al. 2007; Metzger et al. 2008).

An alternative model of central engines of GRBs is newly, rapidly rotating neutron stars or magnetars (Usov 1992; Kluźniak & Ruderman 1998; Dai & Lu 1998; Ruderman et al. 2000; Wheeler et al. 2000). In recent years, newborn neutron stars have also been suggested as an origin of some GRBs and their afterglows. For example, Dai et al. (2006) argued that the X-ray flares discovered by *Swift* can be explained as being due to magnetic instability and reconnection-driven events from highly-magnetized millisecond pulsars; the shallow decay phase of X-ray afterglows is considered to be due to energy injection to a forward shock by a relativistic pulsar wind (Dai 2004; Yu & Dai 2007); a newly-formed neutron star rather than a black hole is expected to explain the light curve of SN 2006aj associated with GRB 060218 (Mazzali et al. 2006; Soderberg et al. 2006). Moreover, simulations on the merger of a compact object binary show that it is possible to form a hypermassive neutron star, at least a transiently existing neutron star after the merger, depending on initial conditions of the binary, equations of state of neutron matter and the structure of magnetic fields (Shibata et al. 2003; Shibata 2003; Lee & Ramirez-Ruiz 2007; Anderson et al. 2008; Liu et al. 2008). Therefore, the hyperaccreting disk around a neutron star can also be considered as possible central engines for some GRBs. Based on these motivations, we have studied the structure of the hyperaccretion disk around a neutron star using both analytic and numerical methods (Zhang & Dai 2008, hereafter ZD08). We found that the neutron-star disk can cool more efficiently and produce a higher neutrino luminosity than the black-hole disk.

In ZD08, the quasi-steady disk around a neutron star is approximately divided into two regions — inner and outer disks, depending on the energy transfer and emission in the disk. For the outer disk, the heating energy rate Q^+ is mainly due to local dissipation ($Q^+ = Q_{\text{vis}}^+$),

and the structure of the outer disk is very similar to the black-hole disk. On the other hand, the heating energy in the inner disk includes both the energy generated by itself and the energy advected from the outer region ($Q^+ = Q_{\text{vis}}^+ + Q_{\text{adv}}^+$), so the inner disk has to be dense with a high pressure. We approximately take $Q^+ = Q^-$ and the entropy-conservation self-similar condition $ds=0$ to describe the inner disk. The size of the inner disk is determined by the global energy equation of the inner disk. However, we need to point out that the entropy-conversation structure is not the only possible structure of the inner disk, which depends on the detailed form of energy and mass transfer. In the case where $Q^- < Q^+$ in the inner disk, we should take the advection-dominated self-similar structure to describe the inner disk.

The net gravitational binding energy of the accreting matter is proposed to drive a relativistic outflow or jet by two general mechanisms that could provide energy for GRBs: neutrino annihilation and magnetohydrodynamical mechanisms such as the Blandford-Znajek effect. The mechanism of neutrino annihilation is easy to understand and could be calculated based on the structure and neutrino luminosity in the disk (Ruffert et al. 1997, 1998; Popham et al. 1999; Asano & Fukuyama 2000, 2001; Di Matteo et al. 2002; Miller et al. 2003; Birkel et al. 2007; Gu et al. 2006; Liu et al. 2007). However, the annihilation rate due to neutrino emission from the black-hole disk may not be able to produce a sufficiently high luminosity to explain some energetic GRBs (Di Matteo et al. 2002). Gu et al. (2006) and Liu et al. (2007) showed that the annihilation luminosity can reach $10^{52} \text{ergs s}^{-1}$ even for an accretion rate $\sim 10 M_{\odot} \text{ s}^{-1}$. However, such an accretion rate is too large for energetic long GRBs, since this requires an unreasonable massive accretion disk around a compact object. As the neutron-star disk structure and neutrino luminosity are different from the black-hole disk, it is interesting to calculate the neutrino annihilation rate above the neutron-star disk and to consider whether the annihilation energy rate and luminosity above a neutron-star disk are high enough to produce energetic GRBs.

On the other hand, we do not consider any outflow from the disk and neutron star in ZD08, which may play a significant role in the structure and energy transfer in the disks around neutron stars. A nonrelativistic or mildly relativistic outflow or “wind” from the disk can be considered as an energy source of supernovae (MacFadyen & Woosley 1999; Kohri et al. 2005). This theoretical model becomes more attractive after the discovery of the connection between some GRBs and supernovae (e.g. Galama et al. 1998, Stanek et al. 2003, Prochaska et al. 2004, Campana et al. 2006), while the GRB component is considered from a relativistic jet produced by neutrino annihilation. As a result, both outflow ejection and neutrino annihilation could be important in the events of GRB-SN connections within the framework of the collapsar model (Woosley & Bloom 2006). However, an outflow from the black-hole disk is expected and becomes important whenever the accretion flow is an

advection-dominated accretion flow (ADAF) (Narayan & Yi 1994, 1995), while the neutrino luminosity is relatively low for ADAF. In other words, neutrino emission may not provide a sufficiently high amount of energy for GRBs associated with supernovae if a thermally-driven outflow is produced from the advection-dominated disk at the same time. Therefore, we need to calculate the neutrino luminosity and annihilation efficiency of the advection-dominated disk with outflow around a neutron star if the neutrino luminosity is much higher for the advection-dominated neutron-star disk than the black-hole disk.

In this paper we still consider the case in which the central object is a neutron star rather than a black hole. Our purpose is to further study the structure of a hyperaccreting neutron-star disk following ZD08, and calculate the neutrino annihilation rate above such a disk. This paper is organized as follows. In §2 we introduce basic equations of the neutrino-cooled disk. We discuss the properties of the inner disk in §3 based on the two-region disk scenario introduced in ZD08. We study the disk with different values of the viscosity parameter α and the energy parameter ε (some quantities are given in this paper in Table 1), and then study the disk structure with an outflow. Two models of an outflow driven from the neutron-star disk are introduced in §3.4. In §4, we calculate the neutrino annihilation rate and luminosity above the neutron-star disk in various cases, and compare the results with the black hole disk. We discuss the effect of the neutrino luminosity at the neutron star surface boundary layer on the annihilation rate. In §5, we particularly focus on an astrophysical application of the neutron-star disk in GRBs and GRB-SN connections. Conclusions are presented in §6.

2. Basic Equations

2.1. Conservation equations

In this paper, all quantities are used as their usual meanings (see ZD08). We adopt the cylindrical coordinates (r, φ, z) to describe the disk. v_r , v_φ are the radial and rotational velocity, Ω is the angular velocity, and Ω_K is the Keplerian angular velocity. $\Sigma = 2\rho H$ is the disk surface density with ρ as the density and H as the half-thickness of the disk. Vertical hydrostatic equilibrium gives $H = c_s/\Omega_K$, where the isothermal sound speed is $c_s = (P/\rho)^{1/2}$ with P to be the gas pressure. The $\nu_k = \alpha c_s H$ is the kinematic viscosity coefficient in the disk with α to be the viscosity parameter.

The mass continuity equation is

$$\frac{1}{r} \frac{d}{dr} (r \Sigma v_r) = 2\dot{\rho} H, \quad (1)$$

where $\dot{\rho}$ is the mass-loss term. If the outflow of the disk is weak, the mass accretion rate \dot{M} can be considered as a constant and we have the accretion rate,

$$\dot{M} = -4\pi r \rho v_r H \equiv -2\pi r \Sigma v_r. \quad (2)$$

In §3.3 we will also discuss the disk structure with outflows.

The angular momentum conservation reads

$$\Sigma r v_r \frac{d(rv_\phi)}{dr} = \frac{d}{dr} \left(\Sigma \alpha \frac{c_s^2}{\Omega_K} r^3 \frac{d\Omega}{dr} \right) + \frac{d}{dr} \dot{J}_{ext}, \quad (3)$$

with \dot{J}_{ext} as the external torque acted on the disk, such as the torque acted by the outflow from the disk. The angular momentum flows into the central compact star or the coupling exerted by the star on the inner edge of the disk is $\dot{C} = -\dot{M}(GM r_*)^{1/2}$ with r_* being the neutron star radius (Frank et al. 2002). Therefore, for a weak outflow, combined with equation (1) and the above boundary condition, equation (3) is integrated as

$$\nu \Sigma = \frac{\dot{M}}{3\pi} \left(1 - \sqrt{\frac{r_*}{r}} \right), \quad (4)$$

where r_* is the neutron star radius. Here we adopted the standard assumption that the torque is zero at the inner boundary of the disk $r_* + b$ with $b \ll r_*$. In §3.3 we will discuss the angular momentum equation with outflow.

The energy equation of the disk is

$$\Sigma v_r T \frac{ds}{dr} = Q^+ - Q^-, \quad (5)$$

where T is the temperature in the disk and s is the local entropy per unit mass, Q^+ and Q^- are the heating and cooling energy rates in the disk. In the outer disk, the energy input is mainly due to the local viscous dissipation,

$$Q^+ = Q_{vis}^+ = \frac{3GM\dot{M}}{8\pi r^3} \left(1 - \sqrt{\frac{r_*}{r}} \right). \quad (6)$$

The left term of equation (5) can be taken as the energy advection term Q_{adv}^- . We can obtain (ZD08)

$$Q_{adv}^- = \Sigma v_r T \frac{ds}{dr} = v_r T \frac{\Sigma}{2r} \left[\frac{R}{2} (1 + Y_e) + \frac{4}{3} g_* \frac{aT^3}{\rho} \right], \quad (7)$$

where $R = 8.315 \times 10^7 \text{ ergs mole}^{-1} \text{ K}^{-1}$ is the gas constant, Y_e is the ratio of electron to nucleon number density, the free degree factor g_* is 2 for photons and 11/2 for a plasma of photons and relativistic e^-e^+ pairs.

The energy cooling rate Q^- is mainly due to neutrino emission, i.e., $Q^- \approx Q_\nu^-$ (Popham & Narayan 1995; Di Matteo et al. 2002),

$$Q_\nu^- = \sum_{i=e,\mu,\tau} \frac{(7/8)\sigma_B T^4}{(3/4)[\tau_{\nu_i}/2 + 1/\sqrt{3} + 1/(3\tau_{a,\nu_i})]}. \quad (8)$$

The three types of neutrino cooling rate per unit volume are

$$\dot{q}_{\nu_e} = \dot{q}_{\text{eN}} + \dot{q}_{e^-e^+ \rightarrow \nu_e \bar{\nu}_e} + \dot{q}_{\text{brem}} + \dot{q}_{\text{plasmon}}, \quad (9)$$

$$\dot{q}_{\nu_\mu} = \dot{q}_{\nu_\tau} = \dot{q}_{e^-e^+ \rightarrow \nu_\tau \bar{\nu}_\tau} + \dot{q}_{\text{brem}}, \quad (10)$$

where \dot{q}_{eN} , $\dot{q}_{e^-e^+ \rightarrow \nu_i \bar{\nu}_i}$, \dot{q}_{brem} , and \dot{q}_{plasmon} are the electron-positron pair capture rate, the electron-positron pair annihilation rate, the nucleon bremsstrahlung rate, and the plasmon decay rate. Following Kohri et al. (2005), Janiuk et al. (2007) and Liu et al. (2007), we calculate the absorption and scattering optical depth for three types of neutrinos $\tau_{a,\nu_i(e,\mu,\tau)}$ and $\tau_{s,\nu_i(e,\mu,\tau)}$ as well as the neutrino cooling rates. For hyperaccretion disks, the electron-positron pair capture rate plays the most important role among several types of neutrino cooling rates.

Moreover, besides the local energy equation (5), we need the global energy conservation equation of the inner disk in order to decide the size of the inner disk. The maximum power that the inner disk can release is estimated as (ZD08)

$$\begin{aligned} L_{\nu,max} &\approx \frac{3GM\dot{M}}{4} \left\{ \frac{1}{3r_*} - \frac{1}{r_{\text{out}}} \left[1 - \frac{2}{3} \left(\frac{r_*}{r_{\text{out}}} \right)^{1/2} \right] \right\} \\ &\quad - \bar{f}_\nu \frac{3GM\dot{M}}{4} \left\{ \frac{1}{\tilde{r}} \left[1 - \frac{2}{3} \left(\frac{r_*}{\tilde{r}} \right)^{1/2} \right] - \frac{1}{r_{\text{out}}} \left[1 - \frac{2}{3} \left(\frac{r_*}{r_{\text{out}}} \right)^{1/2} \right] \right\} \\ &\approx \frac{3GM\dot{M}}{4} \left\{ \frac{1}{3r_*} - \frac{\bar{f}_\nu}{\tilde{r}} \left[1 - \frac{2}{3} \left(\frac{r_*}{\tilde{r}} \right)^{1/2} \right] \right\}, \end{aligned} \quad (11)$$

where \tilde{r} is the radius between inner and outer disks (i.e., the size of the inner disk), the average neutrino cooling efficiency \bar{f}_ν is determined by

$$\bar{f}_\nu = \frac{\int_{\tilde{r}}^{r_{\text{out}}} Q_\nu^- 2\pi r dr}{\int_{\tilde{r}}^{r_{\text{out}}} Q^+ 2\pi r dr}. \quad (12)$$

Thus we derive

$$\int_{r_*}^{\tilde{r}} Q_\nu^- 2\pi r dr = \varepsilon L_{\nu,max} = \varepsilon \frac{3GM\dot{M}}{4} \left\{ \frac{1}{3r_*} - \frac{\bar{f}_\nu}{\tilde{r}} \left[1 - \frac{2}{3} \left(\frac{r_*}{\tilde{r}} \right)^{1/2} \right] \right\} \quad (13)$$

with the energy parameter ε being introduced to measure the neutrino cooling efficiency of the inner disk. When the outer disk flow is mainly an ADAF, we have $\bar{f}_\nu \sim 0$ and the maximum energy release rate of the inner disk to be $G\dot{M}/4r_*$. When the outer disk flows is an efficiently NDAF, then $\bar{f}_\nu \simeq 1$ and the energy release of the inner disk mainly results from the heat energy generated by itself. The values of \bar{f}_ν are calculated analytically in Zhang (2009, Fig. 3.6). In ZD08, we simply set $\varepsilon = 1$ and use the entropy-conservation self-similar structure to describe the inner disk. In §3, we also discuss the case of $\varepsilon < 1$ with different structures of the inner disk. In addition, if we consider an outflow ejected from the disk, equation (13) should be modified. We will discuss the modification in §3.3.

2.2. Pressure and β -equilibrium

The total pressure in the disk is the summation of four terms: nucleons, radiation, electrons (including e^+e^- pairs) and neutrinos,

$$P = P_{\text{nuc}} + P_{\text{rad}} + P_e + P_\nu, \quad (14)$$

where the pressures of nucleons, radiation and electrons are

$$P_{\text{nuc}} = \frac{\rho k_B T}{m_B}, \quad (15)$$

$$P_{\text{rad}} = \frac{1}{3}aT^4, \quad (16)$$

$$P_{e^\pm} = \frac{1}{3} \frac{m_e^4 c^5}{\pi^2 \hbar^3} \int_0^\infty \frac{x^4}{\sqrt{x^2 + 1}} \frac{dx}{e^{(m_e c^2 \sqrt{x^2 + 1} \mp \mu_e)/k_B T} + 1}, \quad (17)$$

and

$$P_e = P_{e^-} + P_{e^+}. \quad (18)$$

We use the Fermi-Dirac distribution to calculate the pressure of electrons, where μ_e is the chemical potential of electron gas, and k_B is the Boltzmann constant.

The ratio of the neutrino pressure to the total pressure becomes noticeable only in very opaque regions of the disk (e.g., Kohri et al. 2005, their Fig. 6; Liu et al. 2007, their Fig. 3). The neutrino pressure is

$$P_\nu = u_\nu/3, \quad (19)$$

where u_ν is the energy density of neutrinos. We adopt the expression of u_ν from previous work (e.g., Di Matteo et al. 2002).

The adiabatic index of the accreting matter is important to determine the size of the inner disk when it satisfies the entropy-conservation condition. It can be written as

$$\gamma = 1 + (P_{\text{nuc}} + P_{\text{rad}} + P_e + P_\nu)/(u_{\text{nuc}} + u_{\text{rad}} + u_e + u_\nu). \quad (20)$$

Moreover, we need the equation of charge neutrality

$$n_p = \frac{\rho Y_e}{m_B} = n_{e^-} - n_{e^+}, \quad (21)$$

and the chemical equilibrium equation

$$\begin{aligned} & n_p(\Gamma_{p+e^- \rightarrow n+\nu_e} + \Gamma_{p+\bar{\nu}_e \rightarrow n+e^+} + \Gamma_{p+e^- + \bar{\nu}_e \rightarrow n}) \\ &= n_n(\Gamma_{n+e^+ \rightarrow p+\bar{\nu}_e} + \Gamma_{n \rightarrow p+e^- + \nu_e} + \Gamma_{n+\nu_e \rightarrow p+e^-}) \end{aligned} \quad (22)$$

to determine the matter components in the disk, where n_p , n_{e^-} and n_{e^+} are the number densities of protons, electrons and positrons, and the various weak interaction rates $\Gamma_{p \rightarrow n}$ ($\Gamma_{n \rightarrow p}$) can be calculated following Janiuk et al. (2007; see also Kawanaka & Mineshige 2007). When neutrinos are perfectly thermalized, we derive the β -equilibrium distribution in the disk

$$\ln \left(\frac{n_n}{n_p} \right) = f(\tau_\nu) \frac{2\mu_e - Q}{k_B T} + [1 - f(\tau_\nu)] \frac{\mu_e - Q}{k_B T}, \quad (23)$$

with $Q = (m_n - m_p)c^2$, and the factor $f(\tau_\nu) = \exp(-\tau_\nu)$ combines the formula from the neutrino-transparent limit case with the the neutrino-opaque limit case of the β -equilibrium distribution. However, we should keep in mind that the β -equilibrium is established only if the neutronization timescale t_n is much shorter than the accretion timescale t_a in the disk $t_n < t_a$. Beloborodov (2003) found that the equilibrium requires the accretion rate \dot{M} to satisfy

$$\dot{M} > \dot{M}_{eq} = 2.24 \times 10^{-3} (r/10^6 \text{cm})^{13/10} (\alpha/0.1)^{9/5} (M/M_\odot)^{-1/10} M_\odot s^{-1}. \quad (24)$$

When the accretion rate is sufficiently low, the electron fraction Y_e would freeze out from weak equilibrium, while the disk becomes advection-dominated (e.g., Metzger et al. 2008b, 2009). In this case, the chemical composition of the disk is determined by its initial condition before its evolution. Metzger et al. (2009), for example, showed that the hyperaccreting disk around a black hole generically freeze out with the fixed $Y_e \sim 0.2 - 0.4$. We will discuss the effect of chemical equilibrium on neutron-star disks more detailedly in the next section. The β -equilibrium assumption can be approximately adopted in our calculations even for the ADAF case.

3. Properties of the Disk

The two-region disk scenario in ZD08 allows the gravitational energy of the neutron-star disk system to be released in three regions: outer disk, inner disk and neutron-star surface. The inner disk region is formed due to the prevention effect of the neutron-star surface, i.e., most advection energy generated in the disk still need to be released in a region near the neutron-star surface. Moreover, a difference between the angular velocity of the neutron-star surface and that of the disk inner boundary layer leads to neutrino emission in the surface boundary layer. In ZD08, we assume all the advected energy to be released in the disk and furthermore all the advected energy from the outer region to be released in the inner disk. Actually, it is possible that a part of the advected energy can be transferred onto the neutron-star surface and finally cooled by neutrino emission from the surface boundary layer rather than the inner disk. Local microphysics quantities such as the inner energy density, neutrino cooling rate, heating convection and conduction properties as well as the advection and cooling timescales should be calculated in order to simulate the inner disk formation and the cooling efficiency of the steady-state inner disk. In this paper, however, we adopt a simple method to determine the inner disk structure, i.e., we use the global energy equation (13) with the global parameter ε instead of the local energy equation (5). The inner disk can release all the advected energy transferred inward for $\varepsilon = 1$, while a part of the advected energy can still be transferred onto the neutron-star surface for $\varepsilon < 1$. Moreover, we approximately take ε as a constant in the inner disk, and adopt the self-similar treatment to calculate the inner disk structure. We take $Q^- = Q^+$ or the entropy-conservation condition $ds = 0$ for $\varepsilon = 1$ in the entire inner disk, and $Q^- = \varepsilon Q^+$ for $\varepsilon < 1$ with the advection-dominated self-similar structure.

With the energy parameter ε in the global energy equation (13) and the self-similar treatment, the inner disk model can be simplified and calculated by assuming the accretion rate, the mass of the central compact object, and the self-similar structure of the inner disk. We discussed the disk structure with the entropy-conservation condition in ZD08, and in this section we further discuss the properties of the neutron-star disk in various cases. Furthermore, we need to consider the effect of an outflow from the neutron-star disk.

3.1. Entropy-Conservation Inner Disk with Different α

The viscosity parameter α was first used by Shakura & Sunyaev (1973) to express the relation between viscous stress $t_{r\theta}$ and the pressure P in the disk as $t_{r\theta} = \alpha P$. Another formula introduces the turbulent kinematic viscosity is $\nu_k = \alpha c_s H$ (Frank et al. 2002). MHD instability simulations show a wide range of α from 0.6 to about 0.005 or less (Hawley

et al. 1995; Brandenburg et al. 1995; Balbus & Hawley 1998; King et al. 2007). King et al. (2007) summarized observational and theoretical estimates of the disk viscosity parameter α . They showed that there is a large discrepancy between the typical values of α from the best observational evidence ($\alpha \sim 0.1 - 0.4$ for fully ionized thin disks) and those obtained from numerical MHD simulations ($\alpha \leq 0.02$ and even considerably smaller). More elaborate numerical simulations should be carried out for resolving this problem. For neutrino-cooled hyperaccreting disks, many previous papers choose $\alpha = 0.1$ as the most typical value. The disk structure with α from 0.01 to 0.1 was discussed in Chen & Beloborodov (2007). On the other hand, hyperaccreting disks with very low α have also been discussed. For example, Chevalier (1996) studied the neutrino-cooled disk with an extremely small $\alpha \sim 10^{-6}$. In this section, we discuss the neutron-star disk with different α . We choose the value of α from 0.001 to 0.1. The size of the inner disk alters with different α , and we still adopt the entropy-conservation self-similar condition of the inner disk to study the effects of the viscosity parameter.

As discussed in ZD08, from equation (13), if $\varepsilon \simeq 1$, the heating energy advected from the outer disk together with the energy generated in the inner disk is totally released in the inner disk, and the energy balance can be established between heating and cooling in the inner disk, i.e., $Q^+ = Q^-$, or from equation (5), $Tds/dr = 0$. In the case where $v_r \ll v_K$ and $\Omega \sim \Omega_K$ but $|\Omega - \Omega_K| \geq v_r/r$, we can obtain the entropy-conservation self-similar structure of the inner disk (Medvedev & Narayan 2001; ZD08) by

$$\rho \propto r^{-1/(\gamma-1)}, \quad P \propto r^{-\gamma/(\gamma-1)}, \quad v_r \propto r^{(3-2\gamma)/(\gamma-1)}. \quad (25)$$

Since the adiabatic index of the accretion matter is not constant, we modify expression (25) as

$$\begin{aligned} \frac{\rho(r)}{\rho(r+dr)} &= \left(\frac{r}{r+dr} \right)^{-1/(\gamma(r)-1)}, \quad \frac{P(r)}{P(r+dr)} = \left(\frac{r}{r+dr} \right)^{-\gamma(r)/(\gamma(r)-1)}, \\ \frac{v(r)}{v(r+dr)} &= \left(\frac{r}{r+dr} \right)^{(3-2\gamma(r))/(\gamma(r)-1)}. \end{aligned} \quad (26)$$

The size of the inner disk \tilde{r} with various α can be determined by equation (13) in §2.1. Figure 1 shows the size of the inner disk as a function of accretion rate with different viscosity parameter $\alpha=0.1, 0.01$ and 0.001 . Same as in ZD08, the outer edge radius of the inner disk \tilde{r} decreases with increasing the accretion rate for a low accretion rate when most part of the disk is advection-dominated. \tilde{r} reaches its minimum value at $\dot{M} \sim 0.1\dot{M}_\odot s^{-1}$ for $\alpha = 0.1$, and then increases with increasing the accretion rate. However, the size of the inner disk becomes smaller for lower viscosity parameter α and would expand dramatically for a higher accretion rate. The characteristic rate \dot{M}_0 which minimizes the size of inner disk \tilde{r}

can be approximated by $\dot{M}_{\text{ch}} \sim \alpha M_{\odot} \text{ s}^{-1}$. The value of accretion rate \dot{M}_{ch} is between those of characteristic rates \dot{M}_{ign} (rate of ignition) and \dot{M}_{opaque} (rate of transparency) in Chen & Beloborodov (2007).

Actually, from ZD08, we derive an approximate analytic equation of the radius \tilde{r} between the inner and outer disks as

$$\tilde{r}^{\frac{5(5-3\gamma)}{4(\gamma-1)}} \left(1 - \sqrt{\frac{r_*}{\tilde{r}}}\right)^{3/4} \left(r_*^{\frac{3\gamma-8}{2(\gamma-1)}} - \tilde{r}^{\frac{3\gamma-8}{2(\gamma-1)}}\right) \propto \dot{M}^{-3/2} \alpha_{-1}^{5/2} \quad (27)$$

for a radiation-pressure-dominated ADAF outer disk, and

$$\left(1 - \sqrt{\frac{r_*}{\tilde{r}}}\right)^{-31/11} \tilde{r}^{(\frac{-1}{\gamma-1} + \frac{3}{22})} \left(r_*^{\frac{2-3\gamma}{\gamma-1}} - \tilde{r}^{\frac{2-3\gamma}{\gamma-1}}\right)^{-1} \propto \dot{M}^{10/11} \alpha_{-1}^{-21/11} \quad (28)$$

for a gas-pressure-dominated ADAF. In both cases, the inner disk size declines as the accretion rate increases or the viscosity parameter α decreases. For a neutrino-dominated disk, the inner disk size \tilde{r} reaches its minimum value

$$\left(\frac{\gamma-1}{3\gamma-2}\right) \tilde{r}^{\frac{2\gamma-1}{\gamma-1}} \left(1 - \sqrt{\frac{r_*}{\tilde{r}}}\right) \left(r_*^{\frac{2-3\gamma}{\gamma-1}} - \tilde{r}^{\frac{2-3\gamma}{\gamma-1}}\right) \propto \left\{\frac{1}{r_*} - \frac{3\bar{f}_{\nu}}{\tilde{r}} \left[1 - \frac{2}{3} \left(\frac{r_*}{\tilde{r}}\right)^{1/2}\right]\right\}. \quad (29)$$

The solution of minimum \tilde{r} declines as α decreases because the lower- α disk has a higher value of \bar{f}_{ν} . As a result, the inner disk size \tilde{r} always decrease with decreasing α in the ADAF case. This conclusion is consistent with that of Figure 1.

For simplicity, we here adopt an unified model introduced in §2 to calculate the structure of the disk both in the ADAF and NDAF cases. In particular, we assume that the disk is always in the β -equilibrium state. Let us focus on this equilibrium assumption. Following Beloborodov (2003, i.e., equation [24] in our paper), we plot the characteristic curves of equilibrium with different values of α in the $\dot{M} - \tilde{r}$ plane of Figure 1. The β -equilibrium state can only be established in the right region divided by the corresponding curve. In the left region, as mentioned at the end of §2.2, the weak interaction timescale become longer than the disk evolutionary timescale, and the electron fraction Y_e freezes out with a fixed value. However, based on the analytic and numerical arguments in ZD08, we found that the solutions of disk structure are relatively insensitive to the value of Y_e , and the main results of Figure 1 can still be unchanged for various Y_e . In ZD08, we fixed the value of $Y_e = 1/9$ and $Y_e = 1$ as the two limits. The inner disk size increases slightly with increasing Y_e in the case of ADAF, and the main result (i.e., the “U”-shape curve in the $\dot{M} - \tilde{r}$ plane as the solution of inner disk size) is still kept for both $Y_e = 1/9$ and $Y_e = 1$. Moreover, although larger Y_e leads to slightly lower value of density, temperature and pressure for ADAF, the physical properties of the ADAF disk with low accretion rate beyond equation (24) is close

to each other for the cases of $Y_e = 1/9$ and 1 (ZD08, Fig. 8). Furthermore, if we adopt the equilibrium assumption in the ADAF case, the value of Y_e will actually not deviate dramatically from 0.5 (i.e., ZD08, the right panel of Fig. 7). Therefore, we always take β -equilibrium as an approximation in our calculation.

Figure 2 shows the structure of the disk for a chosen accretion rate $0.04M_\odot s^{-1}$ as a function of radius for three values of α . The disk with lower α is denser and thinner with higher pressure and larger adiabatic index, and has a brighter neutrino luminosity in most part of the disk except for a part of the inner disk region, which satisfies the self-similar structure. A low- α accretion flow with less kinematic viscosity coefficient ν_k requires a higher surface density Σ for a fixed accretion rate compared to a high- α accretion flow. We have listed approximate analytic solutions of accretion flows in various cases in ZD08. We obtain $\rho \propto \alpha^{-1}$, $P \propto \alpha^{-1}$, $H \propto \alpha^0$ for a radiation-pressure-dominated ADAF, $\rho \propto (1 + Y_e)^{-12/11} \alpha^{-8/11}$, $P \propto (1 + Y_e)^{-4/11} \alpha^{-10/11}$, $H \propto (1 + Y_e)^{4/11} \alpha^{-1/11}$ for a gas-pressure-dominated ADAF, $\rho \propto (1 + Y_e)^{-9/5} \alpha^{-13/10}$, $P \propto (1 + Y_e)^{-3/5} \alpha^{-11/10}$, $H \propto (1 + Y_e)^{3/5} \alpha^{1/10}$ for gas-pressure-dominated NDAF. The density and pressure always increase with decreasing α . These results are consistent with those shown in Figure 2. The disk region where is radiation-pressure-dominated is extremely small for low α (eqs. [22] to [25] in ZD08). Also, as for a low- α disk, the electron fraction Y_e is also low, so the disk is thinner compared to the high- α disk for gas-pressure-dominated ADAF and NDAF, although the viscosity parameter contributes an increasing factor $\alpha^{-1/11}$ for the low- α disk with gas-dominated ADAF.

3.2. Advection-Dominated Inner Disks

The entropy-conservation self-similar structure has been used by Medvedev & Narayan (2001) and ZD08 to discuss the global accretion disk structure. However, such a structure is not the only structure for the neutron-star inner disk, as the entropy-conservation condition $Q^+ = Q^-$ can be satisfied only for $\varepsilon \simeq 1$ in equation (13). In the case where $\varepsilon < 1$, i.e., the inner disk can only partly release the heating energy generated by itself and advected from the outer region, a part of the heating energy in the disk should be still advected onto the neutron star surface and released from the surface, and thus the inner disk cannot satisfy the entropy-conservation self-similar structure. In this case, a part of the heating energy is still advected into the inner region until it is released around the neutron star surface. We can approximately take $Q^- = \varepsilon Q^+$ in the inner disk for $\varepsilon \lesssim 1$, and thus the structure of the inner disk can be described by the ADAF self-similar structure (Spruit et al. 1987, Narayan & Yi 1994):

$$\rho \propto r^{-3/2}, \quad P \propto r^{-5/2}, \quad v_r \propto r^{-1/2}. \quad (30)$$

In Figure 3, we show the inner disk size for four values of the energy parameter $\varepsilon=0.9, 0.7, 0.5$ and 0.2 . We still fix $\alpha=0.1$ in this section in order to see the effects of advection in the inner disk with $\varepsilon < 1$ independently. For the similar reason as in §3.1, we also assume the β -equilibrium for both the case of ADAF and NDAF disks. We find that the size of the inner disk becomes smaller for lower ε . This is because more heating energy can be advected onto the neutron star surface, and the inner disk size is small enough to keep energy balance between heating and cooling in the disk.

Compared with the entropy-conservation self-similar structure, the size of the advection-dominated inner disk is much larger for a low accretion rate when most part of the disk is advection-dominated. When the accretion rate is low, the adiabatic index of the accreting matter is $\gamma \simeq 4/3$ and the entropy-conservation self-similar structure (25) can be approximately taken as $\rho \propto r^{-3}$ and $P \propto r^{-4}$, which requires a more dramatic change of density and pressure than those of the advection-dominated inner disk $\rho \propto r^{-3/2}$ and $P \propto r^{-5/2}$. This difference in structure between entropy-conservation and advection-dominated inner disks makes the size of the inner disks be different with each other.

Finally, what we should point out is that the structure of the advection-dominated self-similar inner disk even with $\varepsilon \rightarrow 1$ is different from the entropy-conservation disk with $\varepsilon = 1$, since these two types of self-similar structure are based on different sets of conservation equations. The advection-dominated structure is based on the mass continuity, radial momentum and angular momentum equations, while we do not consider the local energy equation in which $Q^+ = Q_{\text{vis}}^+ + Q_{\text{adv}}^+$ with Q_{adv}^+ to be difficult to determine locally. We only consider the global energy equation (13) to calculate the size and structure of the inner disk. On the other hand, under the energy-conservation condition $Tds = 0$, we can establish the relation $P \propto \rho^\gamma$ from the local energy equation and obtain the self-similar structure (25) with a combination of the mass continuity and the radial momentum and local energy equations (ZD08). However, neither the relation $P \propto \rho^\gamma$ nor the integrated angular momentum equation (4) can be satisfied in the entropy-conservation solution. In other words, the angular momentum transfer in the inner disk with the structure $P \propto \rho^\gamma$ cannot be merely due to the viscosity. We should consider the external torque acted on the disk or the angular momentum redistribution in the inner disk. We will further discuss the entropy-conservation in §5.

3.3. Inner Disks with Outflows

In §3.1 and §3.2, we do not consider outflows, which may have important effects on the structure and energy flux distribution of the entire disk in some cases. Following Narayan

& Yi (1994, 1995) and Medvedev (2004), if the adiabatic index $\gamma < 3/2$, then the Bernoulli constant of the accretion flow is positive and a thermally-driven wind or outflow can be produced from the disk. Therefore, the outflow component can be important in ADAFs. On the other hand, since the accretion rate of the neutron-star disk is very large, it is reasonable to assume that the neutron star, which has a solid surface and is different from the black hole, cannot accumulate all of the accreting matter at once, and thus an outflow could be produced near the neutron star surface and exist in the inner region of the disk.

In this section, we consider the disk structure and neutrino emission in the disk with a thermally-driven outflow. We consider two models depending on two mechanisms. In the first model (hereafter model O1), an outflow is mainly produced in the process of disk matter accreting onto the surface of a neutron star. We assume that only the inner disk produces an outflow and the accretion rate of the outer disk can still be considered as a constant. We take

$$\dot{M}(r) = \dot{M}_0(r/\tilde{r})^s \quad (31)$$

for the inner disk with s to be the outflow index and \dot{M}_0 to be the constant accretion rate in the outer disk. Second, if an outflow is produced by the accretion process in the disk, then we consider that the outflow is produced in the entire disk (hereafter model O2 in this paper), i.e.,

$$\dot{M}(r) = \dot{M}_0(r/r_{out})^s. \quad (32)$$

Strictly speaking, a thermally-driven outflow from the entire disk is expected in the advection-dominated disk but not in the neutrino-dominated disk. The winds from the disks which emit a sufficient high neutrino luminosity are considered to be driven due to neutrino irradiation (Metzger et al. 2008b). We adopt equation (32) for all the disks with a wide range of the accretion rate in model O2 for simplicity, and we also take the index s of the outflow as a constant. The angular momentum equation with an outflow can be written as

$$\Sigma\nu = \frac{1+2s\zeta}{1+2s} \frac{\dot{M}}{3\pi} \left(1 - \sqrt{\frac{r_*}{r}}\right), \quad (33)$$

where ζ describes a difference between outflow velocity $v_{outflow,\phi}$ and accretion-disk velocity v_ϕ : $v_\phi - v_{outflow,\phi} = \zeta v_\phi$. From equation (33), we see that if $s = 0$ or $\zeta = 1$, i.e., there is no outflow or the toroidal velocity of the outflow is zero and no angular momentum is taken away by the outflow, then the angular momentum equation (33) switches back to the common case of equation (4). In this section, we take $\zeta = 0$, i.e., $v_{outflow,\phi} \approx v_{acc,\phi}$ ¹.

¹Here we do not consider the effects of magnetic fields. In fact, the differences in azimuthal velocity and angular momentum between the outflow and accretion inflow could also exist when the accretion flow is

With the outflow in the inner disk, the self-similar structure becomes

$$\rho \propto r^{s-3/2}, \quad P \propto r^{s-5/2}, \quad v_r \propto r^{-1/2}. \quad (34)$$

The energy-conservation equation of the inner disk can be rewritten as

$$\int_{r_*}^{\tilde{r}} Q_\nu^- 2\pi r dr = \varepsilon \left[\int_{r_*}^{\tilde{r}} \frac{9}{8} \nu \Sigma \frac{GM}{r^3} 2\pi r dr + (1 - \bar{f}_\nu) \int_{\tilde{r}}^{r_{out}} \frac{9}{8} \nu \Sigma \frac{GM}{r^3} 2\pi r dr \right], \quad (35)$$

where we still keep the advection parameter ε . For model O1 that the outflows merely exist in the inner disk due to the neutron star surface, using equations (31) and (33), we derive the energy conservation equation (35) as

$$\begin{aligned} \frac{1}{\varepsilon} \left(\int_{r_*}^{\tilde{r}} Q_\nu^- 2\pi r dr \right) &= \frac{3}{4} \left(\frac{1+2s\zeta}{1+2s} \right) \frac{GM\dot{M}_0}{\tilde{r}^s} \\ &\times \left[\frac{1}{1-s} \left(\frac{1}{r_*^{1-s}} - \frac{1}{\tilde{r}^{1-s}} \right) - \frac{r_*^{1/2}}{3/2-s} \left(\frac{1}{r_*^{3/2-s}} - \frac{1}{\tilde{r}^{3/2-s}} \right) \right] \\ &+ (1 - \bar{f}_\nu) \frac{3GM\dot{M}_0}{4\tilde{r}} \left[1 - \frac{2}{3} \left(\frac{r_*}{\tilde{r}} \right)^{1/2} \right] \end{aligned} \quad (36)$$

for $s < 1$, and

$$\begin{aligned} \frac{1}{\varepsilon} \left(\int_{r_*}^{\tilde{r}} Q_\nu^- 2\pi r dr \right) &= \frac{3}{4} \left(\frac{1+2s\zeta}{1+2s} \right) \frac{GM\dot{M}_0}{\tilde{r}} \left\{ \ln \left(\frac{\tilde{r}}{r_*} \right) - 2 \left[1 - \left(\frac{r_*}{\tilde{r}} \right)^{1/2} \right] \right\} \\ &+ (1 - \bar{f}_\nu) \frac{3GM\dot{M}_0}{4\tilde{r}} \left[1 - \frac{2}{3} \left(\frac{r_*}{\tilde{r}} \right)^{1/2} \right] \end{aligned} \quad (37)$$

for $s = 1$. Here we always consider the outflow index $s \leq 1$.

If the outflows exist in the entire disk (model O2), then we have

$$\begin{aligned} \frac{1}{\varepsilon} \left(\int_{r_*}^{\tilde{r}} Q_\nu^- 2\pi r dr \right) &= \frac{3}{4} \left(\frac{1+2s\zeta}{1+2s} \right) \frac{GM\dot{M}_0}{r_{out}^s} \\ &\times \left[\frac{1}{1-s} \left(\frac{1}{r_*^{1-s}} - \frac{\bar{f}_\nu}{\tilde{r}^{1-s}} \right) - \frac{r_*^{1/2}}{3/2-s} \left(\frac{1}{r_*^{3/2-s}} - \frac{\bar{f}_\nu}{\tilde{r}^{3/2-s}} \right) \right] \end{aligned} \quad (38)$$

governed by a magnetic field (B_ϕ, B_z) without strong poloidal component B_r (Xie & Yuan 2008; Bu et al. 2009). The poloidal magnetic field, however, would cause the outflow to co-rotate with the disk out to the Alfvén radius above the disk surface. In this section, we take the outflow to co-rotate with the accretion inflow $v_{outflow, \phi} \approx v_{acc, \phi}$.

for $s < 1$ and

$$\begin{aligned} \frac{1}{\varepsilon} \left(\int_{r_*}^{\tilde{r}} Q_{\nu}^{-} 2\pi r dr \right) &= \frac{3}{4} \left(\frac{1 + 2s\zeta}{1 + 2s} \right) \frac{GM\dot{M}_0}{r_{out}} \\ &\times \left\{ \ln \left(\frac{r_{out}}{r_*} \right) - \bar{f}_{\nu} \ln \left(\frac{r_{out}}{\tilde{r}} \right) + 2 \left[\bar{f}_{\nu} + \left(\frac{r_*}{\tilde{r}} \right)^{1/2} - 2 \right] \right\} \quad (39) \end{aligned}$$

for $s = 1$. We should point out that, since we derive the energy equations (36)-(39) in the disk with outflow using the angular momentum equation (33) rather than the entropy-conservation expression (26), we still use the self-similar structure (34) to calculate the properties of the inner disk and the entire disk in the case of $\varepsilon \simeq 1$ both in models O1 and O2.

The top two panels in Figure 4 show the size of the inner disk with different values of the advection parameter ε . In model O1, the inner disk is larger for a stronger outflow (larger s) with low accretion rate ($< 0.2M_{\odot}s^{-1}$); but for a high accretion rate ($> 0.2M_{\odot}s^{-1}$), the size of the inner disk decreases with increasing the outflow index s . In fact, if the accretion rate is low, the flow of the outer disk is mainly ADAF and $\bar{f}_{\nu} \sim 0$. From equations (36) and (37), most of the energy generated in the outer disk is advected into the inner region, and the inner disk size is mainly determined by the self-similar structure (34), which requires a less dramatic change of density and pressure as functions of radius for higher s or stronger outflow. As a result, the size of the inner disk becomes larger for a stronger outflow. On the other hand, if the accretion rate is high, we have $\bar{f}_{\nu} \sim 1$ in the outer disk, the inner disk size is mainly determined by the heating energy generated in the inner disk, i.e., the first terms of the right-hand side in equations (36) and (37), and a stronger outflow carries away more energy from the disk and allows a smaller size of the inner disk when the accretion rate is sufficiently high.

The bottom two panels in Figure 4 show the inner disk size in model O2 in which an outflow exists in the entire disk. The inner disk structure cannot exist for a high accretion rate ($> 0.4M_{\odot}s^{-1}$) except for the weak outflow case ($s = 0.2$) where the inner disk can exist in some range of a high accretion rate. The change of the inner disk size is significant for a large outflow index s , and even the entire accretion disk can satisfy the self-similar structure (33) for a sufficiently low accretion rate. For a high accretion rate ($> 0.5M_{\odot}s^{-1}$), the outflow can take away enough heating energy from the disk, and a balance between heating and cooling in the entire disk can be built even without an inner disk. In this range of a high accretion rate, the structure of the neutron-star disk in model O2 is very similar to the black hole disk with an outflow (e.g., Kohri et al. 2005).

Figure 5 shows the structure of the disk with different values of the outflow index $s=0.2, 0.6$ and 1 in model O2. We choose the accretion rate $\dot{M} = 0.2M_{\odot} s^{-1}$ and the energy

parameter $\varepsilon=0.8$. The density and pressure in the disk decrease with increasing the outflow strength in the entire disk, and the disk becomes thicker for a stronger outflow. The change of the temperature is not as obvious as that of the density and pressure. Most part of the outer region of the disk will be cooler for a stronger outflow, but the inner disk region can be hotter in order to release the heating energy advected from the outer region of the disk.

We make a brief summary in the end of this section. We propose the inner disk to satisfy the self-similar structure. Table 2 shows the main results in this section. The inner disk satisfies the entropy-conservation self-similar structure as in ZD08 for the energy parameter $\varepsilon \simeq 1$, while it becomes an advection-dominated self-similar region for $\varepsilon < 1$. In outflow model O1, an outflow is produced in the inner disk due to the prevention effect of the neutron star surface, and model O2 suggests that an outflow exists in the entire disk as in Kohri et al. (2005). We discuss the size of the inner disk depending on different structures of the inner disk and outflow and different values of the viscosity parameter.

4. Neutrino Annihilation

4.1. Calculation Method and Surface Boundary Condition

Hyperaccreting black hole disks can convert some fraction of the net accretion energy into the energy of a relativistic outflow or wind by two general mechanisms: neutrino annihilation and magnetohydrodynamical (MHD) effects such as the Blandford-Znajek mechanism or magnetic instabilities. However, for hyperaccretion disks surrounding neutron stars, the energy conversion mechanism is mainly due to the neutrino annihilation for magnetic fields at the neutron star surface $\leq 10^{15} - 10^{16}$ G. We consider the process of pair annihilation $\nu_i + \bar{\nu}_i \rightarrow e^+ + e^-$ as the most important interaction for energy production. As the neutron-star disk is denser, hotter with higher pressure, and has a brighter neutrino luminosity compared with the black-hole disk in most cases, the neutrino annihilation efficiency of the neutron-star disk should be higher than that of the black-hole disk. Moreover, the surface boundary of the neutron star, which carries away gravitational-binding energy by neutrino emission, also makes the neutrino annihilation luminosity of the neutron-star disk be higher than that of the black-hole counterpart.

In this section, we follow the approximate method used by Ruffert et al. (1997, 1998) and Popham et al. (1999) to calculate the neutrino annihilation luminosity, i.e., the vertically-integrated disk is modeled as a grid of cells in two dimensions (r, ϕ) . The symbols $\epsilon_{\nu_i}^k$ and $l_{\nu_i}^k$ are the mean neutrino energy and neutrino radiation luminosity with three different types of neutrino ($i = e, \tau, \mu$) in the cell k , and d_k is the distance from the cell k to a certain spatial

point. The neutrino annihilation at any point above the disk is

$$l_{\nu\bar{\nu}} = \sum_{i=e,\mu,\tau} A_{1,i} \sum_k \frac{l_{\nu_i}^k}{d_k^2} \sum_{k'} \frac{l_{\bar{\nu}_i}^{k'}}{d_{k'}^2} (\epsilon_{\nu_i}^k + \epsilon_{\bar{\nu}_i}^{k'}) (1 - \cos \theta_{kk'})^2 \\ + \sum_{i=e,\mu,\tau} A_{2,i} \sum_k \frac{l_{\nu_i}^k}{d_k^2} \sum_{k'} \frac{l_{\bar{\nu}_i}^{k'}}{d_{k'}^2} \frac{\epsilon_{\nu_i}^k + \epsilon_{\bar{\nu}_i}^{k'}}{\epsilon_{\nu_i}^k \epsilon_{\bar{\nu}_i}^{k'}} (1 - \cos \theta_{kk'}), \quad (40)$$

where the values of the neutrino cross section constants $A_{1,i}$ and $A_{2,i}$ can be seen in Popham et al. (1999). The total neutrino annihilation luminosity above the disk can be integrated as

$$L_{\nu\bar{\nu}} = 2\pi \int_{r_*}^{\infty} dr \int_H^{\infty} l_{\nu\bar{\nu}} r dz. \quad (41)$$

For a neutron-star disk, we should consider both its different structure compared with the black-hole disk and the boundary condition of the neutron star surface layer. The neutrino annihilation luminosity is not only contributed by neutrinos emitted from the disk but also from the neutron star surface layer. The luminosity available to be radiated by the boundary layer at neutron star surface is (Frank et al. 2002)

$$L_s = \frac{1}{4} \dot{M} r_*^2 (\Omega^2 - \Omega_*^2) - G_* r_* \simeq \frac{GM\dot{M}}{4r_*} \left(1 - \frac{\Omega_*}{\Omega}\right)^2, \quad (42)$$

where Ω and Ω_* are the angular velocity of disk inner boundary and neutron star surface respectively, and $G_* \simeq \frac{1}{2} \dot{M} r_*^2 (\Omega - \Omega_*)$ is the viscous torque acting on the accretion disk. Here we only study the vertically integrated disk over a half-thickness (height) H , and take $\Omega > \Omega_*$. As a result, the luminosity is a function of accretion rate \dot{M} and neutron star surface angular velocity Ω_* . In the case where the inner disk satisfies the entropy-conservation self-similar structure, we introduce the efficiency factor η_s to measure the energy emitting from the neutron star surface and rewrite equation (42) as

$$L_s = \eta_s \frac{GM\dot{M}}{4} \left(\frac{1}{r} - \frac{1}{r_{out}} \right). \quad (43)$$

If $\Omega_* \sim \Omega$, we have $\eta_s \sim 0$ and there is no emission from the surface layer; or if $\Omega_* \sim 0$, we have $\eta_s \sim 1$, which satisfies the Virial condition. We consider the energy released from the surface layer is mainly carried away by neutrino emission, and thus the neutrino emission rate and the temperature at the layer are related by

$$Q_{\nu,s} = \frac{\eta_s}{2\pi r_* H_*} \frac{GM\dot{M}}{4} \left(\frac{1}{r_*} - \frac{1}{r_{out}} \right) \sim \frac{7}{8} \sigma_B T^4. \quad (44)$$

In the case where the self-similar inner disk is advection-dominated, we obtain the gravitational energy released by neutrino emission as

$$L_s = \eta_s \frac{GM\dot{M}}{4} \left(\frac{1}{r} - \frac{1}{r_{out}} \right) + (1 - \varepsilon) \frac{GM\dot{M}}{4} \left\{ \frac{1}{r_*} - \bar{f}_\nu \left[1 - \frac{2}{3} \left(\frac{r_*}{\tilde{r}} \right)^{1/2} \right] \right\}, \quad (45)$$

where the second term in the right side of equation (45) is the heating energy advected from the inner disk to the surface boundary layer, and we can further write equation (45) as

$$L_s = (\eta_s + \eta_{s,ADAF}) \frac{GM\dot{M}}{4} \left(\frac{1}{r} - \frac{1}{r_{out}} \right), \quad (46)$$

where we take the equivalent factor $\eta_{s,ADAF}$ to measure the energy advected from the advection-dominated inner disk to the surface boundary. Table 3 shows examples of $\eta_{s,ADAF}$ with different inner disk structures.

When an outflow exists in the disk, the luminosity at the boundary surface is dimmer since the accretion rate near the neutron star surface is lower due to the outflow. We can modify equation (45) by changing the accretion rate \dot{M} to be $\dot{M}_0(r_*/\tilde{r})^s$ for model O1 in §3.3 and $\dot{M}_0(r_*/r_{out})^s$ for model O2.

4.2. Results of Annihilation Luminosity

We calculate the neutrino annihilation luminosity $L_{\nu\bar{\nu}}$ and the total neutrino luminosity L_ν emitted from the disk and neutron star surface. The results of $L_{\nu\bar{\nu}}$ and L_ν depend on the value of the viscosity parameter α , the detailed structure of the inner disk, the strength of the outflow, as well as the neutron star surface boundary condition. We discuss the effects of these various factors in Figure 6 to Figure 9.

Figure 6 shows the total neutrino annihilation luminosity $L_{\nu\bar{\nu},NS}$ and the emission luminosity $L_{\nu,NS}$ of a neutron-star disk with different surface boundary layer conditions ($\eta_s=0$ and 0.5), and we compare them with the results of a black-hole disk. In this figure we take the neutron-star inner disk structure to satisfy the entropy-conservation self-similar structure (26). The total luminosity and annihilation luminosity of the neutron-star disk are brighter than those of a black-hole disk with the same mass and accretion rate. If we study the neutrino annihilation from the entire disk without surface boundary emission ($\eta_s=0$), the difference between $L_{\nu\bar{\nu},NS}$ and $L_{\nu\bar{\nu},BH}$ is more significant for a low accretion rate than for a high accretion rate. We have mentioned the reason in ZD08 that a larger inner disk for a neutron-star disk with a low accretion rate makes the neutrino luminosity much brighter than its black hole counterpart, and the annihilation rate also becomes higher for the neutron-star

disk. For a high accretion rate ($>0.5M_\odot \text{ s}^{-1}$), the effect of neutrino opacity on $L_{\nu,BH}$ and $L_{\nu\bar{\nu},BH}$ also be less than that on $L_{\nu,NS}$ and $L_{\nu\bar{\nu},NS}$. On the other hand, neutrino emission from the neutron star surface boundary layer ($\eta_s=0.5$) makes the annihilation luminosity be more than one order of magnitude higher than that without boundary emission ($\eta_s=0$). $L_{\nu\bar{\nu}}$ reaches $10^{50} \text{ ergs s}^{-1}$ when $\dot{M} \sim 1M_\odot \text{ s}^{-1}$ for a black-hole disk or neutron-star disk with $\eta_s=0$, but only needs $\dot{M} \sim 0.1M_\odot \text{ s}^{-1}$ for a neutron-star disk with the boundary condition $\eta_s=0.5$. Therefore, a lower-spin neutron star with hyperaccreting disk around it could have an obviously higher annihilation efficiency than that of a higher-spin neutron star. We will discuss the neutrino annihilation luminosity of a neutron-star disk in more details in §5.

In Figure 7, we show the total neutrino annihilation luminosity of a neutron star disk with different values of the viscosity parameter $\alpha=0.1, 0.01, 0.001$ and the energy parameter $\varepsilon=0.9, 0.5, 0.1$. The disk with a moderate viscosity parameter ($\alpha=0.01$) has the highest annihilation efficiency and luminosity for a low accretion rate, and the annihilation luminosity from a high- α disk ($\alpha=0.1$) becomes the brightest for an accretion rate $\dot{M} \geq 0.05M_\odot \text{ s}^{-1}$. As discussed in Figure 2, a low- α disk has a brighter neutrino luminosity Q_ν , but it is thinner than a high- α disk. These two competitive factors lead to the annihilation results shown in Figure 7a. Figure 7b shows that the annihilation efficiency increases with increasing ε . This is because the disk with lower ε means more heating energy in the disk to be advected onto the neutron star surface and increases the neutrino luminosity of the surface layer, and the value of $\eta_{s,ADAF}$, which plays an important role in increasing the annihilation efficiency of the entire disk.

Figure 8 shows the total neutrino annihilation luminosity $L_{\nu\bar{\nu}}$ of the disk with an outflow. We consider the results of model O1 in which an outflow only exists in the inner disk due to the neutron star surface and of model O2 in which an outflow exists in the entire disk. The difference in annihilation luminosity with different values of the outflow index s but the same surface boundary condition is not obvious in model O1. However, $L_{\nu\bar{\nu}}$ becomes much dimmer for a high outflow index s in model O2, which means a strong outflow in the entire disk and decreases the neutrino annihilation efficiency significantly.

Furthermore, we study the spatial distribution of the neutrino annihilation luminosity. Figure 9 illustrates the integrated annihilation luminosity per cm distribution

$$2\pi r \int_H^\infty l_{\nu\bar{\nu}} dz \quad (47)$$

for two accretion rates $\dot{M}=0.01M_\odot \text{ s}^{-1}$ and $0.1M_\odot \text{ s}^{-1}$ with different physical structures of the disk. We find that the integrated annihilation luminosity drops dramatically along the disk radius, and a majority of the annihilation energy is ejected from the cylindric region above the disk with $r < 3 \times 10^6 \text{ cm}$. The difference of the integrated luminosity per cm between the

black-hole disk and neutron-star disk is significant for a low accretion rate when the inner entropy-conservation disk is sufficiently large. The luminosity of the neutron-star disk with an advecting inner disk can be about four orders of magnitude higher than its black-hole counterpart, while an outflow makes the annihilation luminosity above the neutron-star disk be lower than that of the black-hole disk.

Compared with the black-hole disk, the neutron-star disk could produce a brighter neutrino flux and more powerful annihilation luminosity. However, the mass-loss rate driven by neutrino-on-baryon absorption reactions (Qian & Woosley 1996) along the polar axis of the neutron-star disk is also significantly higher than its black-hole counterpart. This raises the problem of whether simultaneously more powerful annihilation luminosity and higher mass loss rate could work together to produce a relativistic jet required for the GRB phenomena. For example, a heavily baryon-loaded wind from a new-born neutron star within 100 ms prevents any production of a relativistic jet (Dessart et al. 2009). However, a weaker wind above the polar region and spherical asymmetry of the outflow at late times could make production of a relativistic jet above the stellar pole become possible. We will discuss this issue in more details in §5.3.

5. Discussions

5.1. Size of the Inner Disk

In §3 we study various self-similar structures of the inner disk. In this section we further discuss the entropy-conservation structure. The inner disk can be determined by the self-similar structure (26) and the energy equation (13). However, the inner disk with the entropy-conservation structure cannot satisfy the integrated angular momentum equation (4). There are two explanations. First, we can consider the term $d\dot{J}_{ext}/dr \neq 0$ in equation (3) for a steady-state disk since the angular momentum redistributes in the inner disk before the entire disk becomes steady-state. As mentioned in ZD08, because the neutron star surface prevents heating energy from being further advected inward, the inner disk forms to balance the heating and cooling energy in the entire disk. As a result, energy and angular momentum could redistribute in the inner disk. Second, besides this consideration on angular momentum redistribution, we can also discuss another type of inner disk with the entropy-conservation structure discussed by Medvedev & Narayan (2000), which still satisfies the angular momentum equation (4) with $v_r \ll v_K$ and $\Omega \simeq \text{constant}$. The angular momentum transfer and heating energy generation due to viscosity can be neglected in the inner disk, as Ω is approximately equal to a constant, and the heating energy in the inner disk is merely the energy advected from the outer disk, i.e., $Q^+ = Q_{adv}^+$ in the inner disk. As a result, the

global inner-disk energy conservation equation (13) should be modified as

$$\int_{r_*}^{\tilde{r}} Q_{\nu}^{-} 2\pi r dr = \frac{3GM\dot{M}}{4} \left\{ \frac{1}{3\tilde{r}} - \frac{\bar{f}_{\nu}}{\tilde{r}} \left[1 - \frac{2}{3} \left(\frac{r_*}{\tilde{r}} \right)^{1/2} \right] \right\}, \quad (48)$$

for $\Omega \simeq \text{constant} = \Omega(\tilde{r})$ in the inner disk. Compared with equation (13), equation (48) requires a smaller value of \tilde{r} with the same neutron star mass and accretion rate. Figure 10 shows the value of \tilde{r} for $\alpha=0.1$ and 0.01 with $\Omega \simeq \text{constant}$ and $\Omega \propto r^{-3/2}$. The constant angular velocity in the inner disk decreases the inner disk size compared to the case of $\Omega \propto r^{-3/2}$. However, in order to get a unified scenario of the entire disk in various cases, we adopt $\Omega \propto r^{-3/2}$ for all the self-similar structures in §3.

5.2. Annihilation Results and Disk Geometry

Several previous studies have been performed to calculate the neutrino annihilation efficiency above the disk around a black hole with the effects of disk geometry, gravitational bending, rotation of central black holes and so on (e.g., Ruffert et al. 1997, 1998; Popham et al. 1999; Asano & Fukuyama 2000, 2001; Miller et al. 2003; Birkel et al. 2007). The simulations based on general relativity show the effects of general relativity such as the Kerr black holes and bending neutrino geodesics in spacetime increase the total annihilation rate by a factor of a few. Also, compared with the spherical and torus neutrinosphere, the disk neutrinosphere with the same temperature and neutrino luminosity distribution usually have the highest annihilation efficiency (Birkel et al. 2007). In this paper, we still adopt the calculation approach on annihilation based on Ruffert et al. (1997, 1998) and Popham et al. (1999), and consider the vertically-integrated Newtonian disk. The most important results of annihilation calculation in our work is that the neutron-star disk produce more energetic annihilation luminosity compared to the black-hole counterpart. Moreover, we consider neutrinos emitted from the stellar surface region, and the neutrino emission concentrated in this surface region plays a significant role in increasing the annihilation luminosity to produce relativistic ejecta formed by e^+e^- plasma. On the other hand, we should note that the effect of surface boundary condition emission could be reduced if the emission region becomes larger than we consider in this paper due to outflow or the other cooling mechanisms rather than neutrino cooling at the surface. Some other works focusing on neutrino annihilation in supernovae discussed neutrino emission from the entire spherical neutron star surface (Cooperstein et al. 1986; Goodman et al. 1987; Salmonson & Wilson 1999). Therefore, a further work should be done to study the effects of boundary emission and cooling based on more elaborate considerations on cooling mechanisms and energy transfer at the boundary around neutron-star disk. However, as the neutron-star disk and the surface

emission increase the annihilation luminosity more significantly than the general relativity effects, we conclude our main results would maintain for more elaborate simulations based on advanced calculations on neutrino annihilation above the disk.

5.3. Application to GRB Phenomena

Energy can be deposited in the polar region of black-hole and neutron-star disks by neutrino annihilation and MHD processes. We focus on the annihilation process in this paper. In the black-hole case, the environment along the polar axis (i.e., the rotation axis of the disk around neutron star) can be baryon-free. For example, GRB can commence after the initial collapse for ~ 15 s in the collapsar scenario, when the accretion process in the polar region becomes sufficiently weak to produce a relatively clean environment with the mass density $\leq 10^6$ g cm $^{-3}$ (MacFadyen & Woosley 1999). In the neutron-star case, however, the enormous neutrino luminosity of a neutron star would drive appreciable mass-loss from its surface during the first 20 s of its life (Qian & Woosley 1996). The wind material will feed the polar region, where a large amount of annihilation energy is deposited. Dessart et al. (2009) showed that a newly formed neutron star from the neutron star binary merger will develop a powerful neutrino-driven wind in the polar funnel in a few milliseconds after its formation. The mass-loss associated with the neutrino-driven wind is on the order of $10^{-3}M_{\odot}$ s $^{-1}$, preventing energy outflow from being accelerated to relativistic speed and producing a GRB. Their numerical simulations stops at $t \sim 100$ ms, while they considered that the neutron star will collapse to a black hole quickly. However, a stable neutron star with much longer lifetime $\gg 100$ ms has also been proposed as the GRB central engine. A rapidly rotating neutron star formed by the neutron star binary merger (Gao & Fan 2006) or the merger of a white dwarf binary (King et al. 2001) could produce extended emission (Metzger et al. 2008b) or X-ray flares (Dai et al. 2006) about 10-100 s after the neutron star birth, and last for tens of seconds. In the collapsar scenario, a newly formed neutron star or a magnetar could also form after the initial collapse or associated supernova explosion, and the lifetime of the neutron star before collapsing to a black hole can reach as long as several months to yrs (Vietri & Stella 1998). Therefore, many GRB models lead to a longtime ($\gg 100$ ms) neutron star, which can produce other phenomena accompanying the GRB prompt emission. On the other hand, the accretion timescale can last for longer than 10s in the collapse process of a massive star, or for several seconds after the merger of a compact star binary with the disk viscosity parameter $\alpha < 0.1$ (Narayan et al. 2001). Thus we can discuss the steady-state scenario of a neutron star with lifetime $\gg 100$ ms surrounded by a hyperaccreting disk.

For a longtime neutron star, the strengthen of a neutrino-driven winds above the stellar

polar region would drop quickly at late times, as the total mass-loss rate $\dot{M} \sim t^{-5/3}$, and the neutrino-driven wind become weaker above the polar region than that from the low latitudes and midplane region of the neutron star. It is difficult to calculate the spatial distribution of Lorentz factor of the outflow material above the polar region precisely in our present work, because we only use the approximate disk geometry to calculate the steady-state spatial distribution of the neutrino annihilation efficiency. We do not simulate the dynamical evolution of the neutrino-driven wind. However, we can estimate the speed of outflow material using semi-analytic methods as follows. The mass loss rate for a thermal neutrino-driven wind can be approximately given by (Qian & Woosley 1996)

$$\dot{M}_{\text{wind}} \approx 1.14 \times 10^{-10} C^{5/3} L_{\bar{\nu}_e, 51} \epsilon_{\nu_e, \text{MeV}}^{10/3} (r/10^6 \text{cm})^{5/3} (M/1.4M_\odot)^{-2} M_\odot \text{s}^{-1}, \quad (49)$$

where $10^{51} L_{\bar{\nu}_e, 51} \text{ergs s}^{-1}$ is the luminosity of the $\bar{\nu}_e$ emission, $\epsilon_{\nu_e} = 1 \text{MeV} \epsilon_{\nu_e, \text{MeV}}$ is the mean neutrino energy of the neutron star surface, and $C \approx 1 + 0.733(r/10^6 \text{cm})^{-1} (M/1.4M_\odot)$. Thus the typical steady state spherical mass-loss rate due to thermal neutrino absorption reactions for a neutron star with 10km radius is on the order of a few $10^{-6} - 10^{-5} M_\odot \text{s}^{-1}$, depending on the initial configuration of the material above the neutron star surface (i.e., Qian & Woosley 1996, Tab. 1). The mass-loss rate depends on the neutrino luminosity and temperature above the neutron star surface sensitively. When the neutron star with weak magnetic field $< 10^{15} \text{G}$ is surrounded by a hyperaccreting disk, the neutron star surface should have a higher temperature near the star midplane than its polar region, as mentioned in the last section §4. Thus the neutron star should produce a stronger wind above the midplane region than above its poles. As a result, the mass-loss rate via neutrino absorption above the star polar region is estimated as

$$\dot{M}_{\text{polar}} = \dot{M}_{\text{wind}} \left(\frac{\Delta\Omega}{2\pi} \right) f_{\text{asy}}, \quad (50)$$

where $\Delta\Omega = \int \cos\varphi d\varphi d\phi$ is the solid angle of the polar funnel, and $f_{\text{asy}} < 1$ is used to measure the degree of spherical asymmetry. Moreover, the bulk Lorentz factor of the outflows from the neutron star surface is

$$\Gamma \geq \frac{L_{\nu\bar{\nu}} f_k}{\dot{M}_{\text{polar}} c^2} = \frac{L_{\nu\bar{\nu}}}{\dot{M}_{\text{wind}} c^2} \left(\frac{2\pi f_k}{\Delta\Omega f_{\text{asy}}} \right), \quad (51)$$

where f_k is the fraction of deposited annihilation energy which provides kinetic energy of the neutron star wind above the polar region. We can estimate whether the outflow material from the polar region of the neutron star surface can be accelerated to a relativistic speed using equation (51). Here we take the bulk Lorentz factor $1 < \Gamma < 10$ as a mildly relativistic speed, $10 \leq \Gamma < 100$ as a moderately relativistic speed and $\Gamma > 100$ as an ultrarelativistic speed. If we take the bulk Lorentz factor Γ as a parameter, the solid angle of the polar region

$\Delta\Omega/2\pi \sim 0.1$, and $f_k \sim f_{asy}$, then we can estimate the upper limit of total thermal mass-loss rate from the neutron star surface with particular boundary layer conditions, and compare such limits with the actual mass-loss rate of thermal neutrino-driven winds calculated by equation (49). In Figure 11 we explore the possibility of producing a relativistic jet. We show the maximum allowed strength of total mass-loss for the wind material above the polar region being accelerated to $\Gamma = 10$ and $\Gamma = 100$ with the chosen boundary layer condition $\eta_s = 0$ and $\eta_s = 0.5$ as in §4. The neutrino emission from the neutron star surface layer increases the neutrino annihilation luminosity and efficiency, while it increases the stellar surface mass-loss simultaneously. From Figure 11, we find that moderately relativistic outflows above the neutron star polar region are possible under some cases, e.g., the wind material can be accelerated to $10 < \Gamma < 100$ above the polar region for the disk accretion rate $\dot{M} \geq 0.08M_\odot \text{ s}^{-1}$ with $\eta_s = 0.5$. This result can still be kept for other values of f_k/f_{asy} around unit. However, annihilation process can never produce any winds with bulk Lorentz factor $\Gamma \geq 100$, as the heavily mass-loaded neutron-star wind precludes ultrarelativistic speed even for very high annihilation efficiency with sufficiently bright neutrino emission from the innermost disk radius. Zhang et al. (2003, 2004) found that relativistic jets formed in the accreting black hole systems can be collimated by their passage through the stellar envelope; moderately and even mildly relativistic jets can be partly accelerated to an ultrarelativistic speed after they break out in the massive star, because the jets' internal energy can be converted to kinetic energy after jet breakout. Such jet-stellar-envelope interactions also happen around the hyperaccreting neutron star systems, although the neutron-star disk systems can be surrounded by a cavity $\sim 10^9$ cm inside the progenitor stars with the stellar radius of several 10^{10} cm (e.g., Bucciantini et al. 2008, 2009). In the compact star binary merger scenario, on the other hand, a moderately relativistic jet is possible to produce a short-duration GRB.

As a result, the neutron-star disk can produce a sufficiently larger annihilation luminosity than its black-hole counterpart. However, a neutrino-driven outflow from the newly formed neutron star at early times (~ 100 ms) is so heavily mass-loaded that it can in no way be accelerated to relativistic speed. For a longtime neutron star, however, mass-loss becomes weaker above the stellar pole than above the low latitudes and midplane. Thus a moderately relativistic jet can be produced in a hyperaccreting neutron-star system with sufficiently high disk accretion rate and bright boundary emission (e.g., the accretion rate $\dot{M} \geq 0.08M_\odot \text{ s}^{-1}$ for $\eta_s = 0.5$). Also, the jet can be collimated by jet-stellar-envelope interactions, and partly accelerated to an ultrarelativistic speed after jet breakout if the neutron star forms through stellar collapse. Therefore, some hyperaccreting neutron-star system can produce GRBs, which are more energetic than those from the black-hole systems. We know that some long-duration GRBs can reach a peak luminosity of $\sim 10^{52}$ ergs s^{-1} (e.g. GRB 990123, Kulkarni et al. 1999), which requires a very high accretion rate $\sim 10M_\odot \text{ s}^{-1}$ as

well as a much more massive disk ($\geq 10M_\odot$) around a black hole compared to the typical disk or torus mass $0.01 - 1M_\odot$ if the energy is provided by neutrino annihilation above the black-hole disk. However, if we consider the neutron-star disk with the surface boundary emission (e.g. $\eta_s \sim 0.5$), we only need an accretion rate $\sim 1M_\odot \text{ s}^{-1}$ onto the neutron star, which is one order of magnitude less than that of the black-hole disk, and the disk mass can be $\sim 1M_\odot$ for a long burst with the peak luminosity $10^{52} \text{ ergs s}^{-1}$ in a time of about 1s. However, other reasons or mechanisms such as the jet effect to reduce the total burst energy or the magnetic mechanism rather than neutrino annihilation to provide the GRB energy have been introduced into the GRB central engine models. Therefore, it is necessary to search new important observational evidence to show the existence of a central neutron star rather than black hole surrounded by a hyperaccreting disk. X-ray flares after GRBs may be a piece of evidence, which shows that an activity of the central neutron star after the burst may be due to magnetic instability and reconnection effects in differentially-rotating pulsars (Dai et al. 2006). However, more studies should be done to compare other models of X-ray flares (King et al. 2005; Proga & Zhang 2006; Perna et al. 2005; Lee & Ramires-Ruiz 2007, Lazzati et al. 2008) with the differential-rotating pulsar model and show more effects of such a magnetized pulsar. For example, the spin-down power of a magnetar probably explains the peculiar optical to X-ray integrated luminosity of GRB 060218 (Soderberg et al. 2006).

Furthermore, we propose that other GRB-like events may be produced by hyperaccreting neutron star systems, if winds fail to reach a proper relativistic speed. As mentioned by MacFadyen et al. (2001), a mildly or moderately relativistic jet may lead to X-ray flashes, which are less energetic than normal GRBs. This will also happen in the neutron-star case. Another possible result is that a heavily mass-loaded wind with nonrelativistic speed could produce a bright SN-like optical transient event (Kohri et al. 2005; Metzger et al. 2008a).

5.4. GRB-SN Association

Besides GRBa and GRB-like phenomena, we think a nonrelativistic or mildly relativistic outflow from a hyperaccreting disk and neutron star surface may feed a supernova explosion associated with a GRB. The discovery of connection between some GRBs and supernovae has inspired studies of the origin of GRB-SN association (e.g., Iwamota et al. 1998; MacFadyen & Woosley 1999; Zhang et al. 2004; Nagataki et al. 2006, 2007; Mazzali et al. 2006). As discussed in Kohri et al. (2005), an outflow from the hyperaccreting disk is possible to provide a successful supernova with both prompt explosion or delayed explosion. Therefore, it is reasonable to propose a general scenario for the origin of GRB-SN connection: some

hyperaccreting disks with outflows around compact objects are central engines of GRBs or XRFs accompanied by supernovae. The thermal-driven outflow energy from the disk provides a part of or even a majority of the kinetic energy of a supernova, and neutrino annihilation from the disk provides the energy of a GRB if the accretion rate is sufficiently high. Now we use the results in §3.3 and §4.2 to discuss the energy of the outflow from the disk, and compare it with the neutrino annihilation luminosity and energy above the disk. The upper limit of the energy rate carried away by the outflow can be estimated by subtracting the heating energy rate generated in the disk from the ideal heating energy rate of the disk without outflow, i.e., the maximum energy rate of the outflow is

$$\dot{E}_{o,max} \sim \frac{3GM\dot{M}}{4} \left\{ \frac{1}{3r_*} - \frac{1}{r_{out}} \left[1 - \frac{2}{3} \left(\frac{r_*}{r_{out}} \right)^{1/2} \right] \right\} - \int_{r_*}^{r_{out}} \frac{9}{8} \nu \Sigma \frac{GM}{r^3} 2\pi r dr, \quad (52)$$

and the total actual outflow energy can be considered to be $\sim 0.1-1$ fraction of the maximum outflow energy. In Table 4 we list various energy rates, including the heating energy rate in the disk, the maximum energy injection rate to an outflow and the neutrino annihilation rate above the disk. We choose the accretion rate to be $0.3M_\odot \text{ s}^{-1}$ in both models O1 and O2 in §3.3. Compared with model O1, the neutron-star disk with an outflow from the entire disk (model O2) produces higher outflow energy but less neutrino annihilation rate. If the disk mass around a neutron star is $\sim 1M_\odot$, then the maximum outflow energy is $\sim 10^{51}$ ergs in model O1, and $\sim 10^{52}$ ergs in model O2, but the annihilation luminosity in model O2 would be one or two orders of magnitude less than that in model O1. Besides the case of a neutron star, the black-hole disk with an outflow can provide the same order of outflow energy ejecta as in model O2, but even dimmer annihilation luminosity than model O2. Therefore, further studies of an energy relation between GRBs and supernovae in GRB-SN events could distinguish between the neutron-star disk models (model O1 and O2) and the black-hole disk model.

5.5. Effects of Magnetic Fields

In this paper, we do not consider the effect of magnetic fields. As mentioned in ZD08, the high magnetic fields of central neutron stars or magnetars $> 10^{15} - 10^{16} \text{ G}$ could play a significant role in the global structure of the disk as well as various microphysical processes in the disk. Moreover, compared to the neutron star surface, which produces e^+e^- jets and outflows, the central magnetars could be considered as a possible source to produce magnetically-dominated outflows and collimated jets with ultrarelativistic bulk Lorentz factors (e.g., Usov 1992; Lyutikov 2006; Uzdensky & MacFadyen 2007; Tchekhovskoy et al. 2008; Metzger et al. 2008a, Bucciantini et al. 2008, 2009). For example, Bucciantini et al.

(2008, 2009) modeled the interaction between the wind from a newly formed rapidly rotating protomagnetar and the surrounding progenitor. The free-flowing wind from protomagnetar is not possible to achieve simultaneously collimation and acceleration to high Lorentz factor. However, a bubble of relativistic plasma and a strong toroidal magnetic field created by the magnetar wind shocking on the surrounding stellar envelope can work together to drive a relativistic jet, which is possible to produce a long GRBs and the associated Type Ic supernova. Metzger et al. (2008a) showed that protomagnetars are capable to produce neutron-rich long GRB outflows for submillisecond rotation period $P \leq 0.8$ ms. Besides the study on the central magnetar, the properties of magnetized NDAF disk has also been studied. Recently Lei et al. (2009) investigated the properties of the NDAF with the magnetic torque acted between the central black hole and the disk. The neutrino annihilation luminosity can be increased by one order of magnitude higher for accretion rate $\sim 0.5M_{\odot} \text{ s}^{-1}$, and the disk becomes thermally and viscously unstable in the inner region. Therefore, it is also interesting to study the effects of ultra-highly magnetic fields of neutron stars or magnetars on hyperaccreting disks.

6. Conclusions

In this paper we have studied the structure of a hyperaccreting disk around a neutron star based on the two-region scenario, and calculate the neutrino annihilation luminosity above the disks with different structures. The neutron-star disk model is still Newtonian, vertically-integrated with one-dimensional variable radius r , and based on the α -prescription. The accretion rate \dot{M} is the basic quantity to determine the properties of the disk and the annihilation luminosity, and we also discuss the effects of the energy parameter ε of the inner disk (eqs. [13], [35] to [39]), the viscosity parameter α , the outflow structure and strength (eqs. [31], [32]), the neutrino emission for the stellar surface layer to increase the total annihilation energy rate (eqs. [42] to [46]).

We adopt the self-similar structure to describe the inner disk, in which the heating mechanism is different from the outer disk. Table 2 shows the inner disk structure and size in various cases depending on the value of ε and the properties of the outflow from the disk. We introduce two disk outflow models in §3.3. In model O1, we consider the outflow is mainly from the inner disk, while model O2 suggests that an outflow exists in the entire disk. In §5.1, we also discuss the other possibilities of the entropy-conservation self-similar structure of the inner disk.

Compared to a high- α disk ($\alpha \sim 0.1$), the size of a low- α disk is smaller for a low accretion rate ($\leq 0.1M_{\odot} \text{ s}^{-1}$) and increases dramatically with increasing accretion rate (Fig.

1). A low- α disk is denser, thinner with higher pressure and larger adiabatic index, and has a brighter neutrino luminosity (Fig. 2). The size of the inner disk which satisfies the advection-dominated self-similar structure for $\varepsilon < 1$ becomes smaller for lower ε , and is much larger compared to the entropy-conservation inner disk for a low accretion rate ($\leq 0.1M_{\odot} \text{ s}^{-1}$, Fig. 3). In outflow model O1, the inner disk is larger for a stronger outflow with low accretion rate, but its size decreases with increasing the outflow index s for a high accretion rate. Moreover, the inner disk would not exist in outflow model O2 when the accretion rate $\geq 0.5M_{\odot} \text{ s}^{-1}$ (Fig. 4). The outflow in the entire disk decreases the density and pressure, but increases the thickness of the disk (Fig. 5).

The neutrino annihilation luminosity above the neutron-star disk $L_{\nu\bar{\nu},NS}$ is higher than the black-hole disk $L_{\nu\bar{\nu},BH}$, and the difference between $L_{\nu\bar{\nu},NS}$ and $L_{\nu\bar{\nu},BH}$ is significant for a low accretion rate due to the different disk structure and neutrino luminosity between them (Fig. 6). The neutrino emission from the neutron star surface boundary layer is produced in the process of disk matter accreting onto the surface, and the boundary emission can increase the total neutrino annihilation rate above the disk significantly for about one order of magnitude higher than the disk without boundary emission (Fig. 6, Fig. 7, Fig. 8). The disk with an advection-dominated inner disk could produce the highest neutrino luminosity while the disk with an outflow from the entire disk (model O2) produces the lowest annihilation luminosity (Fig 7, Fig 8, Fig 9). We show that the annihilation luminosity can reach $10^{52} \text{ ergs s}^{-1}$ when the accretion rate $\sim 1M_{\odot} \text{ s}^{-1}$ for neutron-star disks, while the higher accretion rate $\sim 10M_{\odot} \text{ s}^{-1}$ is needed to reach $10^{52} \text{ ergs s}^{-1}$ for black-hole disks. Therefore, the neutron-star disk can produce a sufficiently large annihilation luminosity than its black-hole counterpart. Although a heavily mass-loaded outflow from the neutron star surface at early times of neutron star formation prevents the outflow material from being accelerated to a high bulk Lorentz factor, an energetic relativistic jet can be produced above the stellar polar region at late times if the disk accretion rate and the neutrino emission luminosity from the surface boundary are sufficiently high. Such relativistic jet may be further accelerated by jet-stellar-envelope interaction and produce the GRB or GRB-like events such as X-ray flashes (XRFs).

The outflow from the advection-dominated disk and low latitudes of the neutron star surface can be considered to provide the energy and sufficient ^{56}Ni for successful supernova explosions associated with GRBs or XRFs in some previous works. However, the energy produced via neutrino annihilation above the advection-dominated black-hole disk is usually not sufficient for relativistic ejecta and GRBs. On the other hand, the advection-dominated disk around a neutron star can produce a much higher annihilation luminosity compared to the black-hole disk. Outflow model O2 produces a higher neutrino annihilation rate but less outflow energy compared to model O1, while the black-hole disk could provide

the same order of outflow energy but even less annihilation energy compared to model O2. Therefore, observations on GRB-SN connection would further constrain these models between hyperaccreting disks around black holes and neutron stars with outflows.

Acknowledgements

We would like to thank the anonymous referee for his/her very useful comments that have allowed us to improve our paper significantly. This work is supported by the National Natural Science Foundation of China (grants 10221001, 10640420144 and 10873009) and the National Basic Research Program of China (973 program) No. 2007CB815404.

REFERENCES

- Anderson, M., et al. 2008, *Phys. Rev. Lett.*, 100, 191101
- Asano, K., & Fukuyama, T. 2000, *ApJ*, 531, 949
- Asano, K., & Fukuyama, T. 2001, *ApJ*, 546, 1019
- Balbus, S. A., & Hawley, J. F. 1998, *Rev. Mod. Phys.*, 70, 1
- Beloborodov, A. M. 2003, *ApJ*, 588, 931
- Birkel, R., Aloy, M. A., Janka, H.-T., & Müller, E. 2007, *A&A*, 463, 51
- Brandenburg, A., Nordlund, A., Stein, R. F., & Torkelsson, U. 1995, *ApJ*, 446, 741
- Bu, D. F., Yuan, F. & Xie, F.-G. 2009, *MNRAS*, 392, 325
- Bucciantini, N. et al. 2008, *MNRAS*, 383, 25
- Bucciantini, N. et al. 2009, *MNRAS*, 396, 2038
- Campana, S., et al., 2006, *Nature*, 442, 7106
- Chen, W., & Beloborodov, A. M. 2007, *ApJ*, 657, 383
- Chevalier, R. A. 1996, *ApJ*, 459, 322
- Cooperstein, J., van den Horn, L. J., & Baron, E. A. 1986, *ApJ*, 309, 653
- Dai, Z. G. 2004, *ApJ*, 606, 1000

- Dai, Z. G., & Lu, T. 1998, *Phys. Rev. Lett.*, 81, 4301
- Dai, Z. G., Wang, X. Y., Wu, X. F., & Zhang, B. 2006, *Science*, 311, 1127
- Dessat, L. et al. 2009, *ApJ*, 690, 1681
- Di Matteo, T., Perna, R., & Narayan, R. 2002, *ApJ*, 579, 706
- Eichler, D., Livio, M., Piran, T., & Schramm, D. N. 1989, *Nature*, 340, 126
- Frank, J., King, A., & Raine, D. 2002, *Accretion Power in Astrophysics* (Cambridge: Cambridge Univ. Press)
- Gao, W. H., & Fan, Y. Z. 2006, *ChJAA*, 6, 513
- Hawley, J. F., Gammie, C. F., & Balbus S. A. 1995, *ApJ*, 440, 742
- Iwamoto, K., et al., 1998, *Nature*, 395, 672
- Janiuk, A., Yuan, Y., Perna, R., & Di Matteo, T. 2007, *ApJ*, 664, 1011
- Kawanaka, N., & Mineshige, S. 2007, *ApJ*, 662, 1156
- King, A. R., Pringle, J. E., & Wickramasinghe, D. T. 2001, *MNRAS*, 320, 45
- King, A. R., et al. 2005, *ApJ*, 630, L113
- King, A. R., Pringle, J. E., & Livio, M. 2007, *MNRAS*, 376, 1740
- Kluźniak, W., & Ruderman, M. 1998, *ApJ*, 505, L113
- Kulkarni, S. R. et al. 1999, *Nature*, 398, 389
- Kohri, K., & Mineshige, S. 2002, *ApJ*, 577, 311
- Kohri, K., Narayan, R., & Piran, T. 2005, *ApJ*, 629, 341
- Lazzati, D., Perna, R., & Begelman, M. C. 2008, *MNRAS*, 388, 15
- Lee, W. & Ramirez-Ruiz, E. 2007, *New J. Phys.*, 9, 17
- Lei, W. H., et al. 2009, *ApJ*, accepted, astro-ph/0906.1635
- Liu, T., Gu, W. M., Xue, L., & Lu, J. F. 2007, *ApJ*, 661, 1025
- Liu, Y. T., Shapiro, S. L., Etienne, Z. B., & Taniguchi, K. 2008, *Phys. Rev. D.*, 68, 024012

- Lyutikov, M. 2006, *New Journal of Physics*, 8, 119
- Goodman, J., Dar, A., & Nussinov, S. 1987, *ApJ*, 314, L7
- Galama, T. J., et al., 1998, *Nature*, 395, 670
- Gu, W.-M., Liu, T., & Lu, J.-F. 2006, *ApJ*, 643, L87
- MacFadyen, A. I., & Woosley, S. E. 1999, *ApJ*, 524, 262
- MacFadyen, A. I., Woosley, S. E., & Heger, A. 2001, *ApJ*, 550, 410
- Mazzali, P. A. et al. 2006, *Nature*, 442, 1018
- Medvedev, M. V., & Narayan, R. 2001, *ApJ*, 554, 1255
- Medvedev, M. V. 2004, preprint (astro-ph/0407062)
- Metzger, B. D., Thompson, T. A., & Quataert, E. 2008a, *ApJ*, 676, 1130
- Metzger, B. D., Piro, A. L., & Quataert, E. 2008b, *MNRAS*, 390, 781
- Metzger, B. D., Piro, A. L., & Quataert, E. 2009, *MNRAS*, 396, 304
- Miller, W. A., George, N. D., Hhefets, A., & McGhee, J. M. 2003, *ApJ*, 583, 833
- Nagataki, S., Mizuta, A., & Sato, K. 2006, *ApJ*, 647, 1255
- Nagataki, S., Takahashi, R., Mizuta, A., & Takiwaki, T. 2007, *ApJ*, 659, 512
- Narayan, R., Paczyński, B., & Piran, T. 1992, *ApJ*, 395, L83
- Narayan, R., Piran, T., & Kumar, P. 2001, *ApJ*, 557, 949
- Narayan, R., & Yi, I. 1994, *ApJ*, 428, L13
- Narayan, R., & Yi, I. 1995, *ApJ*, 444, 231
- Paczynski, B. 1998, *ApJ*, 494, L45
- Perna, R., Armitage, P. J., & Zhang, B. 2005, *ApJ*, 636, L29
- Popham, R., Woosley, S. E., & Fryer, C. 1999, *ApJ*, 518, 356
- Prochaska, J. X., et al., 2004, *ApJ*, 611, 200
- Proga, D. & Zhang, B. 2006, *MNRAS*, 370, L61

- Qian, Y.-Z. & Woosley, S. E. 1996, *ApJ*, 471, 331
- Ruderman, M. A., Tao, L., Kluźniak, W. 2000, *ApJ*, 542, 243
- Ruffert, M., Janka, H.-T., Takahashi, K., & Schaefer, G. 1997, *A&A*, 319, 122
- Ruffert, M., & Janka, H.-T. 1998, *A&A*, 338, 535
- Salmonson, J. D., & Wilson, J. R. 1999, *ApJ*, 517, 859
- Shakura, N. I., & Sunyaev, R. A. 1973, *A&A*, 24, 337
- Shibata, M. 2003, *Phys. Rev. D*. 67, 024033
- Shibata, M., Taniguchi, K., & Uryū, K. 2003, *Phys. Rev. D.*, 68, 084020
- Soderberg, A. M. et al. 2006, *Nature*, 442, 1014
- Spruit, H. C., Matsuda, T., Inoue, M., & Sawada, K. 1987, *MNRAS*, 229, 517
- Stanek, et al. 2003, *ApJ*, 591, L17
- Tchekhovskoy, A., McKinney, J. C., & Narayan, R. 2008, *MNRAS*, 388, 551
- Usov, V. V. 1992, *Nature*, 357, 472
- Uzdensky, D. A., & MacFadyen, A. I. 2007, *ApJ*, 669, 546
- Vietri, M., & Stella, L. 1998, *ApJ*, 507, 45L
- Wheeler, J. C., Yi, I., Hoffich, P., & Wang, L. 2000, *ApJ*, 537, 810
- Woosley, S. E. 1993, *ApJ*, 405, 273
- Woosley, S. E., & Bloom, J. S. 2006, *ARA&A*, 44, 507
- Xie, F.-G., & Yuan, F. 2008, *ApJ*, 681, 499
- Yu, Y. W., & Dai, Z. G. 2007, *A&A*, 470, 119
- Zhang, D. 2009, Master thesis, astro-ph/0906.0842
- Zhang, D., & Dai, Z. G. 2008, *ApJ*, 683, 329 (ZD08)
- Zhang, W., Woosley, S. E., & MacFadyen, A. I. 2003, *ApJ*, 586, 356
- Zhang, W., & Woosley, S. E. 2004, *ApJ*, 608, 365

This preprint was prepared with the AAS L^AT_EX macros v5.2.

Notation and definition of some quantities in this paper

notation	definition	§/Eq.
ε	energy parameter	§2.1, eq.(13)
γ	adiabatic index of the accreting matter	§2.2, eq.(20)
s	outflow index	§3.3, eq.(31)
ζ	toroidal velocity difference between outflow and accretion disk	§3.3, eq.(33)
η_s	efficiency factor to measure the surface emission	§4.1, eq.(43)
$\eta_{s,ADAF}$	efficiency factor to measure the energy advected from the disk	§4.1, eq.(46)

Table 1:

Self-similar structure and size of the inner disk in various cases		
Cases	Inner disk self-similar structure	Inner disk size
Case 1: $\varepsilon \simeq 1$, no outflow	entropy-conservation structure (26)	Figure 1
Case 2: $\varepsilon < 1$, no outflow	advection-dominated structure (30)	Figure 3
Case 3: outflow model O1	outflow structure (34)	Figure 4 top panels
Case 4: outflow model O2	outflow structure (34)	Figure 4 bottom panels

Table 2: We discuss case 1 in §3.1, case 2 in §3.2, case 3 and case 4 in §3.3 with different inner disk structures based on energy and mass transfer in the entire disk.

Equivalent factor $\eta_{s,ADAF}$ with different inner disk structures						
$\eta_{s,ADAF}$	0.03	0.1	0.3	0.5	1.0	3.0
	$(M_{\odot} \text{ s}^{-1})$					
$\varepsilon=0.9$	9.07e-2	5.25e-2	4.22e-2	5.56e-2	7.75e-2	9.56e-2
$\varepsilon=0.5$	0.419	0.196	0.159	0.149	0.180	0.446
$\varepsilon=0.2$	0.675	0.496	0.219	0.178	0.218	0.382
O1: $s=0.2$	0.228	0.113	7.84e-2	8.72e-2	0.107	0.202
$s=0.6$	–	0.215	0.115	0.113	0.119	0.209
$s=1.0$	–	0.315	0.199	0.168	0.203	0.336
O2: $s=0.2$	0.238	0.104	7.95e-3	–	–	–
$s=0.6$	–	0.428	5.79e-4	–	–	–
$s=1.0$	–	–	0.639	4.36e-4	–	–

Table 3: Equations (45) and (46) give the value of $\eta_{s,ADAF}$. We choose cases of the advection-dominated inner disk with $\varepsilon=0.9, 0.5, 0.2$, and models O1 and O2 with $s=0.2, 0.6, 1.0$ to calculate $\eta_{s,ADAF}$.

Comparison of energy rates between outflow and neutrino annihilation				
Cases	disk heating rate ($10^{51}\text{ergs s}^{-1}$)	max outflow energy rate ($10^{51}\text{ergs s}^{-1}$)	$L_{\nu\bar{\nu}}$ ($\eta_s=0$) ($10^{51}\text{ergs s}^{-1}$)	$L_{\nu\bar{\nu}}$ ($\eta_s=0.5$) ($10^{51}\text{ergs s}^{-1}$)
model O1: $s=0.2$	25.3	1.09	8.37e-2	2.24
$s=0.6$	24.7	1.72	0.104	1.74
$s=1.0$	18.4	7.95	0.179	1.65
model O2: $s=0.2$	14.6	11.8	1.42e-2	0.522
$s=0.6$	6.50	19.9	4.84e-3	2.54e-2
$s=1.0$	4.07	22.3	3.48e-3	5.99e-3

Table 4: We consider model O1 and O2 with the outflow index $s=0.2, 0.6, 1.0$, the accretion rate $\dot{M} = 0.3M_{\odot} \text{ s}^{-1}$ and the energy parameter $\varepsilon=0.8$.

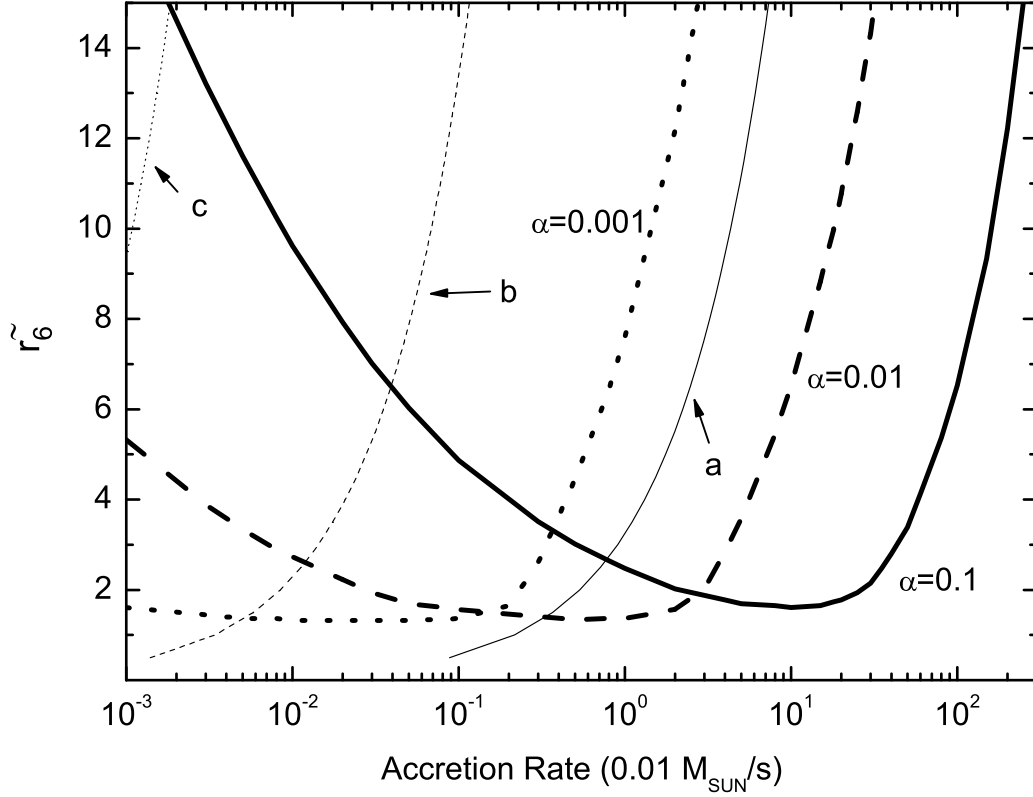


Fig. 1.— The radius \tilde{r} (\tilde{r}_6 , in units of 10^6 cm) of the boundary layer between the inner and outer disks as a function of accretion rate with different values of the viscosity parameter $\alpha=0.1$ (thick solid line), 0.01 (thick dashed line) and 0.001 (thick dotted line). The three thin lines labeled “a”, “b”, and “c” are the characteristic curves of β -equilibrium with three values of $\alpha=0.1$, 0.01 and 0.001 respectively. Each characteristic curve divides the $\dot{M} - \tilde{r}$ parameter plane into two regions with a chosen α , and β -equilibrium can be established in the right region respectively.

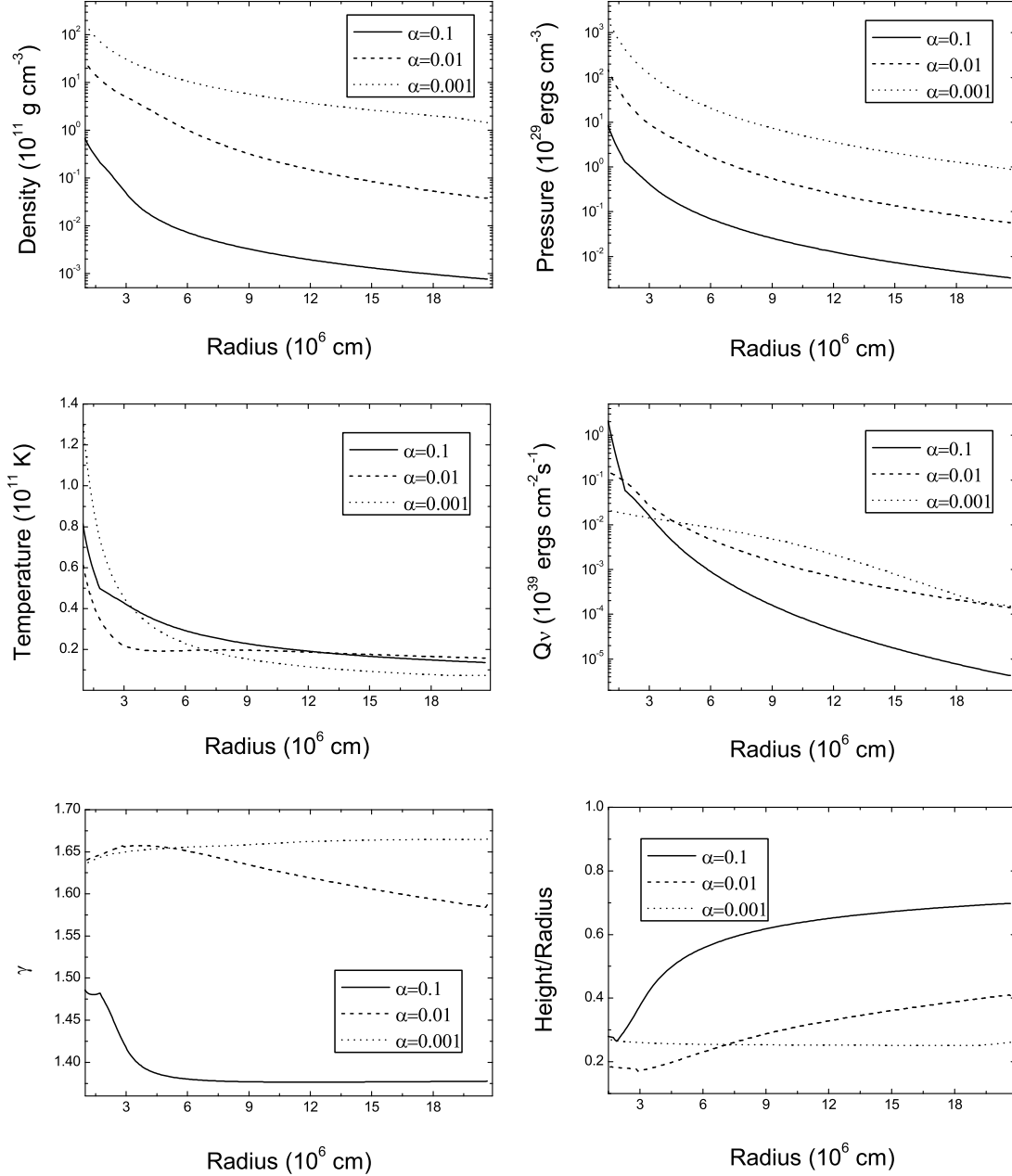


Fig. 2.— The density, pressure, temperature, neutrino luminosity per unit area, adiabatic index γ and height (half-thickness of the disk) of the entire disk with different values of the viscosity parameter $\alpha=0.1$ (solid line), 0.01 (dashed line) and 0.001 (dotted line) with a fixed accretion rate $\dot{M} = 0.04 M_{\odot} \text{ s}^{-1}$.

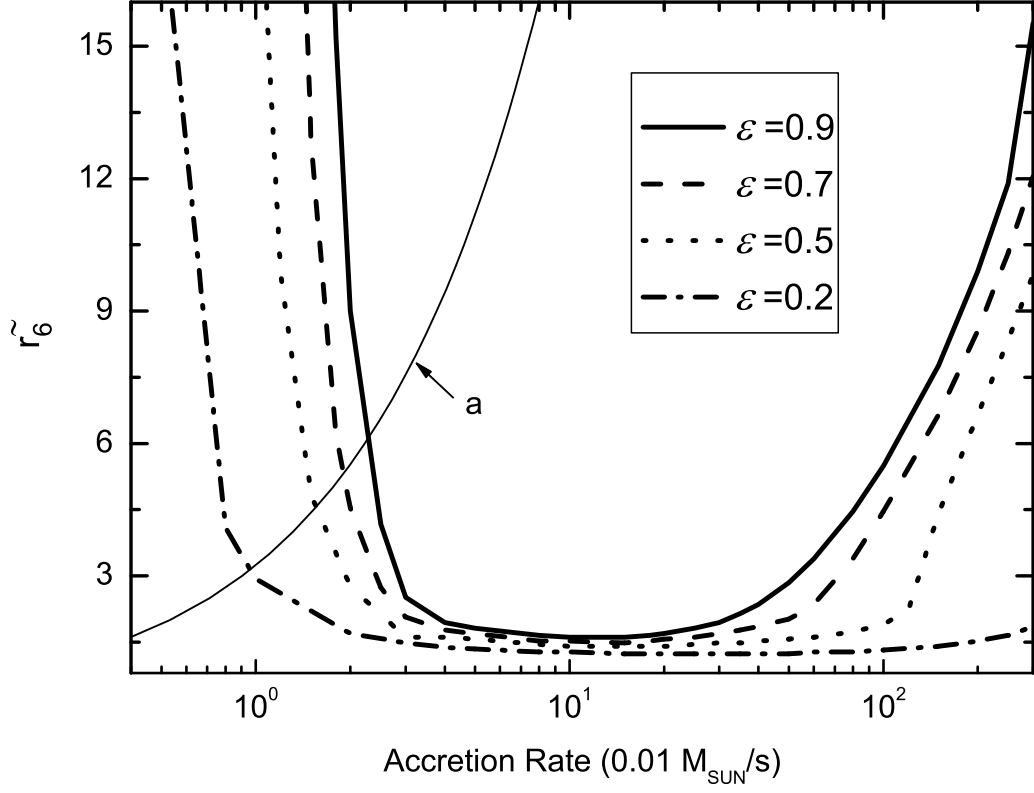


Fig. 3.— The radius \tilde{r} (in units of 10^6 cm) between the inner and outer disks as a function of accretion rate with different values of the energy parameter $\epsilon=0.9, 0.7, 0.5$ and 0.2 . The thin line labeled “a” is the characteristic curve of equilibrium as in Fig. 1 with $\alpha=0.1$.

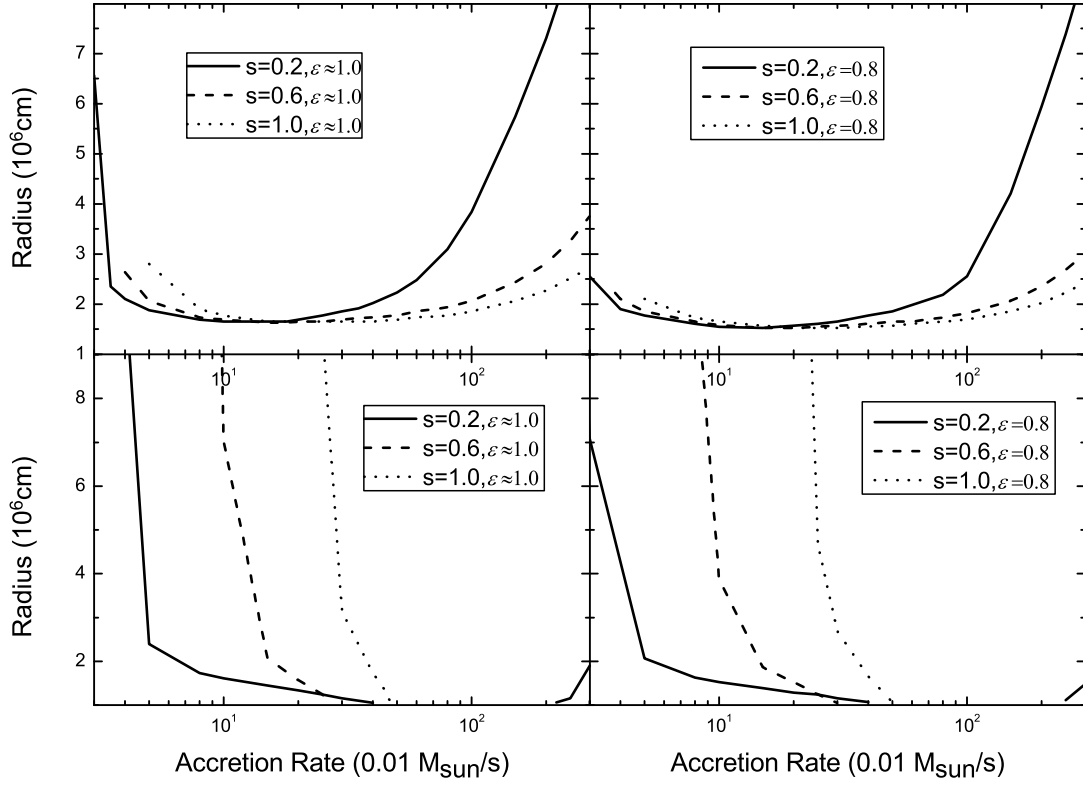


Fig. 4.— (a) *Top panels*: the radius \tilde{r} between the inner and outer disk in model O1 with different parameter sets of the outflow index $s=0.2, 0.6, 1$ and the energy parameter $\varepsilon \simeq 1, 0.8$. (b) *Bottom panels*: the radius \tilde{r} in model O2 with the same parameter sets (s, ε) as in the top two panels.

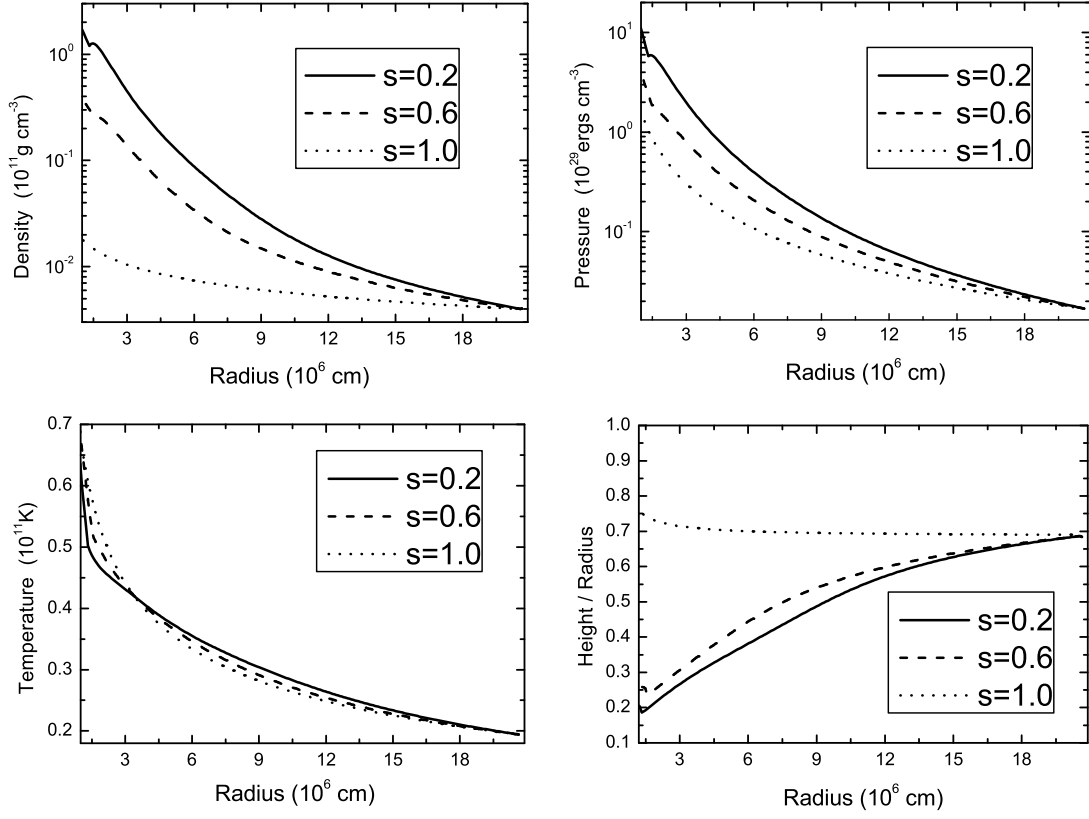


Fig. 5.— Density, pressure, temperature and height (half-thickness) as functions of radius for different values of the outflow index $s=0.2, 0.6, 1$, where we take the accretion rate as $0.2M_{\odot} \text{ s}^{-1}$ and the energy parameter $\varepsilon=0.8$.

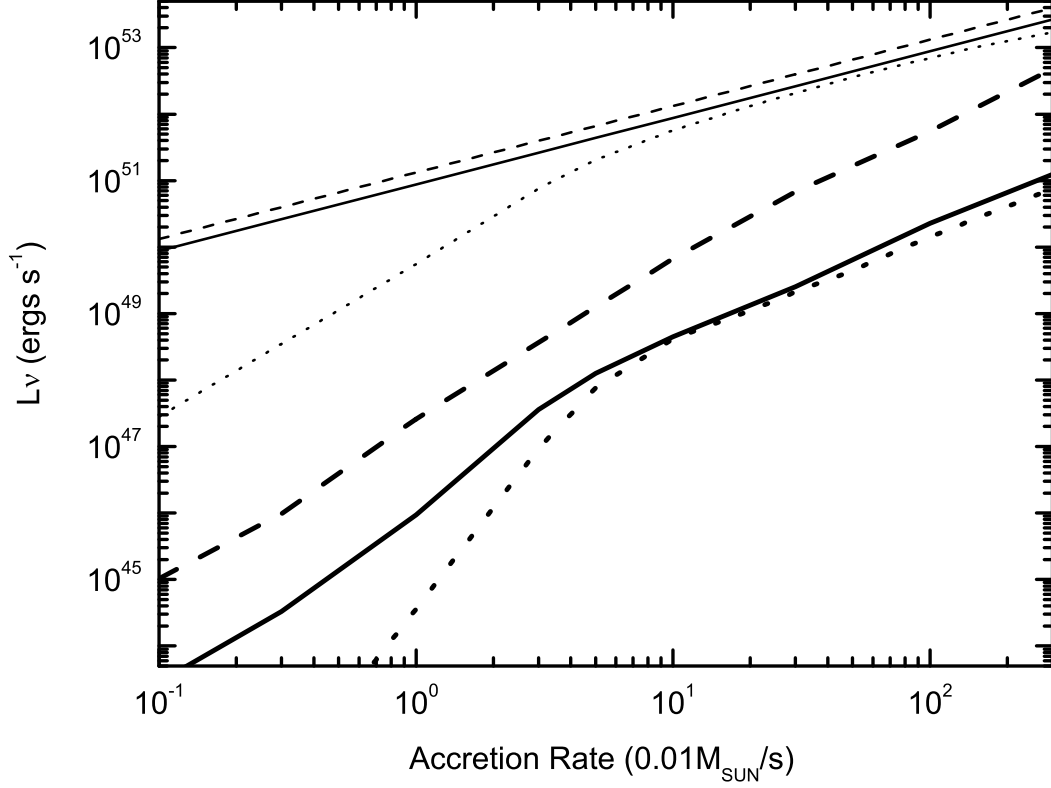


Fig. 6.— Neutrino annihilation luminosity $L_{\nu\bar{\nu}}$ (*thick lines*) and total neutrino emission luminosity L_{ν} (*thin lines*) as functions of accretion rate. The solid lines correspond to the neutron-star disk with the entropy-conservation inner disk and the boundary layer emission efficiency $\eta_s = 0$, the dashed lines to the neutron-star disk with the boundary condition $\eta_s = 0.5$, and the dotted lines to the black-hole disk.

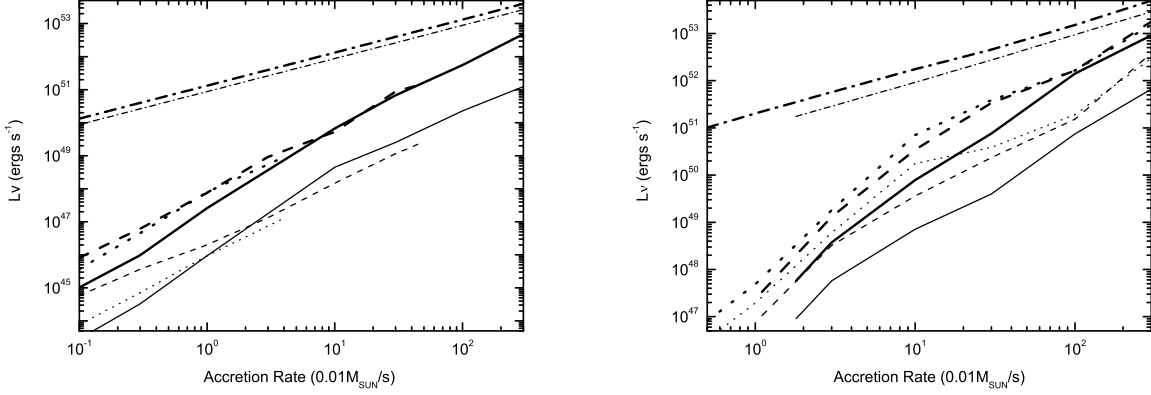


Fig. 7.— Neutrino annihilation luminosity $L_{\nu\bar{\nu}}$ and the total neutrino luminosity L_{ν} with different values of the viscosity parameter α and energy parameter ε . The thin lines correspond to $\eta_s = 0$ and thick lines to $\eta_s = 0.5$. (a) *Left panel*: $L_{\nu\bar{\nu}}$ with $\alpha=0.1$ (solid line), 0.01 (dashed line), 0.001 (dotted line) and total luminosity L_{ν} (dash-dotted line), where we take $\varepsilon = 1$ and the entropy-conservation inner disk structure. (b) *Right panel*: $L_{\nu\bar{\nu}}$ of the neutron-star disk with advection-dominated inner disk and $\varepsilon=0.9$ (solid line), 0.5 (dashed line), 0.1 (dotted line) and the total luminosity L_{ν} (dash-dotted line).

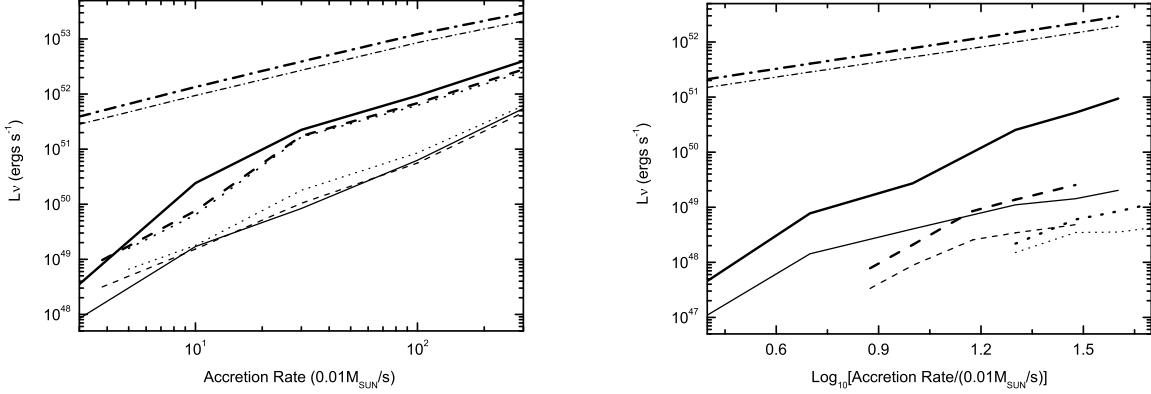


Fig. 8.— Neutrino annihilation luminosity $L_{\nu\bar{\nu}}$ of the neutron-star disk with outflow index $s=0.2$ (solid line), 0.6 (dashed line), 1.0 (dotted line) and the maximum value of total luminosity L_{ν} in the case of $s=0.2$ (dash-dotted line), where we take $\varepsilon=0.8$. Left panel shows the results of model O1 and right panel to model O2. The thin lines correspond to the luminosity to $\eta_s = 0$ and thick lines to $\eta_s = 0.5$.

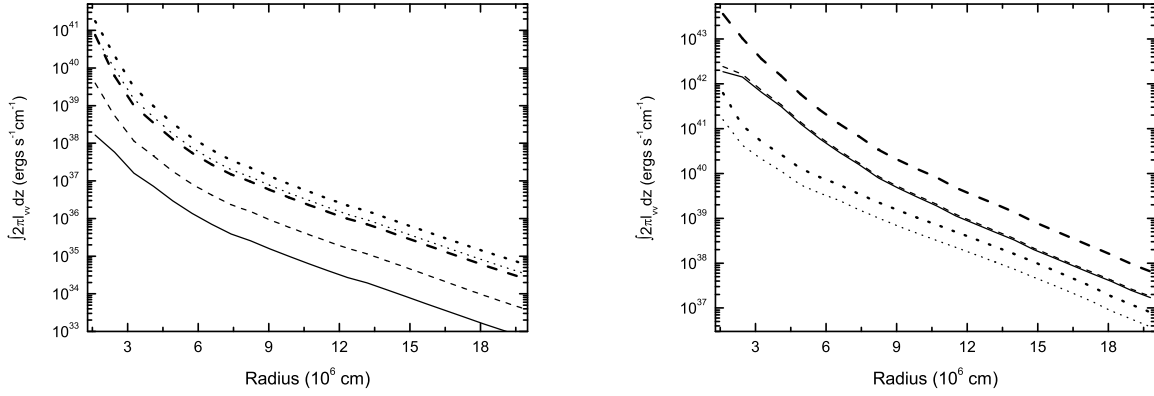


Fig. 9.— Neutrino annihilation luminosity per cm distribution as a function of radius for $\dot{M}=0.01M_{\odot} \text{ s}^{-1}$ (left panel) and $\dot{M}=0.1M_{\odot} \text{ s}^{-1}$ (right panel). (a) *Left panel*: annihilation luminosity per cm for a black-hole disk (*thin solid line*), neutron-star disks with entropy-conservation inner disk and $\eta_s=0$ (*thin dashed line*), and $\eta_s=0.5$ (*thick dashed line*), and neutron-star disks with advection-dominated inner disk $\varepsilon=0.2$ and $\eta_s=0$ (*thin dotted line*), and $\varepsilon=0.2$ and $\eta_s=0.5$ (*thick dotted line*). (b) *Right panel*: annihilation luminosity per cm for a neutron-star disk with outflow (model O2) $\varepsilon=1$, $s=0.6$, $\eta_s=0$ (*thin dotted line*), $\varepsilon=1$, $s=0.6$, $\eta_s=0.5$ (*thick dotted line*). The thin solid line, thin dashed line and thick dashed line are the same as the left panel.

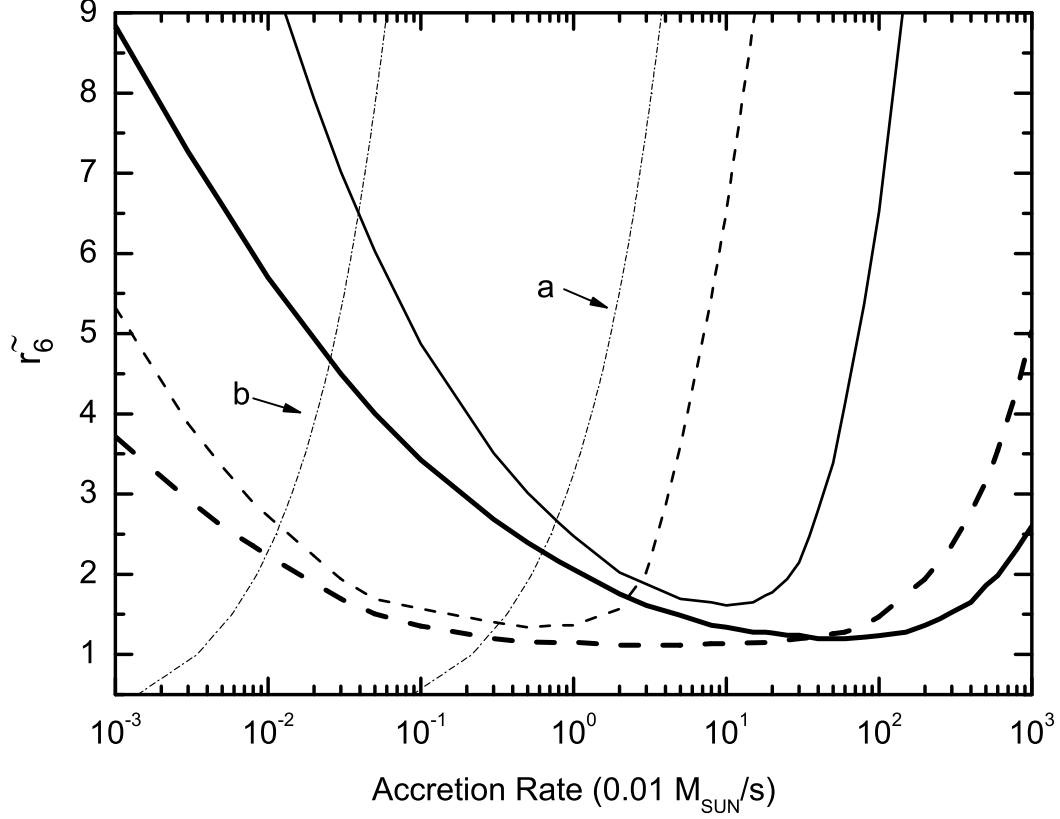


Fig. 10.— The radius \tilde{r} (in units of 10^6 cm) between the inner and outer disks with the viscosity parameter $\alpha=0.1$ (*solid line*) and 0.01 (*dashed line*). The thick lines show the results based on the consideration $\Omega \simeq \text{const}$ in the inner disk in §5, and the thin lines based on the angular velocity distribution $\Omega \propto r^{-3/2}$ as in §3. The dashed-dotted lines “a” and “b” correspond to the characteristic curve of β -equilibrium as in Fig. 1 with the viscosity parameter $\alpha=0.1$ and $\alpha=0.01$.

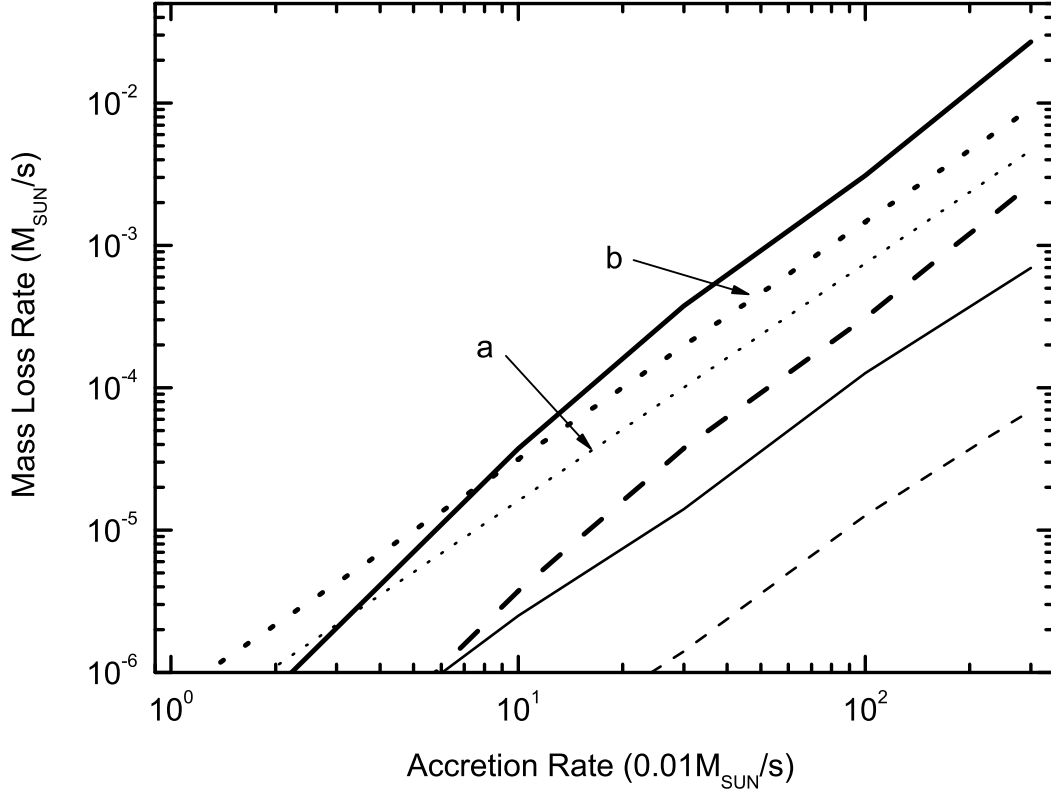


Fig. 11.— Upper limit of mass-loss rate due to neutrino-driven wind from the neutron star surface for the outflow being accelerated to $\Gamma = 10$ (moderately relativistic) with the surface emission boundary condition $\eta_s = 0$ (*thin solid line*) or $\eta_s = 0.5$ (*thin dashed line*); or $\Gamma = 100$ (ultrarelativistic) with the surface emission boundary condition $\eta_s = 0$ (*thick solid line*) or $\eta_s = 0.5$ (*thick dashed line*). The dotted lines “a” and “b” correspond to the strength of a thermally neutrino-driven wind from the stellar surface for the boundary condition $\eta_s = 0$ and $\eta_s = 0.5$ respectively..